# Unfolding long-term Late Pleistocene–Holocene disturbances of forest communities in the southwestern Amazonian lowlands

DILCE F. ROSSETTI [ID],[1],† ROGÉRIO GRIBEL,[2] PETER M. TOLEDO,[1] SONIA H. TATUMI,[3] MÁRCIO YEE,[3]
DIEGO R. G. TUDELA,[4] CASIMIRO S. MUNITA,[5] AND LUIZ DE SOUZA COELHO[2]

[1]Brazilian Institute for Space Research-INPE, Rua dos Astronautas 1758, São José dos Campos, SP 12245–970 Brazil
[2]Coordination of Biodiversity, Brazilian National Institute of Amazonian Research-INPA, Av. André Araújo 2936, Manaus,
AM 69067-375 Brazil
[3]Federal University of São Paulo, Santos, SP 11070-100 Brazil
[4]University of São Paulo, São Paulo, SP 05508900 Brazil
[5]Institute for Nuclear Research, São Paulo, SP 05508900 Brazil

**Abstract.**   Linking the distribution of plant species to geology has generally been biased by the over-simplification of landscape evolution and the lack of understanding of complex geological processes. The Amazonian lowlands have forests in different successional stages, and a growing perception is that such heterogeneity results from long-term environmental changes. This hypothesis is investigated by designing an analytical model based on past and present-day vegetation and successions of the plant communities, combined with an advanced understanding of geological history. An area of southwestern Amazonia was selected for floristic inventories, and we interpreted the paleovegetation based on C/N and $\delta^{13}$C analyses of sedimentary organic matter. These data were examined in the context of the geological evolution on the basis of new sedimentological and chronological data. The topographically high Late Pleistocene deposits had continuous and highly diversified late-successional terra firme forests as well as local fluvial pale-olandforms of younger ages with less diversified campinarana forests. Late Pleistocene–Holocene terrains in intermediate elevations had terra firme forests, but shorter trees with lower basal areas and ecotonal forests appeared near the confines of the forest–savanna, while Holocene deposits recorded only seasonally flooded varzea forests. Several deposits of Late Pleistocene and Late Pleistocene–Holocene age recorded an expansion of $C_4$ terrestrial plants before the establishment of the forest from ~20,000 cal yr BP to 7578 cal yr BP, which is not related to past arid episodes. We recorded forests with onsets at 6130–3533 cal yr BP, 3402–2800 cal yr BP, and 1624–964 cal yr BP to terra firme, varzea, and ecotonal forests, respectively. However, not all forests have reached maturity stages due to their location on terrains with a diverse history of terrace downcutting and deposition, which had a direct impact on local hydrology with the interaction of topographic gradients. The hydrology of the study area was also controlled by the distance from the main river valley. Capturing long-term disturbances over this region of still pristine forests may help elucidate the potential mechanisms that also determine trends in tree growth and forest diversity in other Neotropical regions.

**Key words:**   Amazonian lowlands; distribution patterns; forest onset; geological history; Holocene; Late Pleistocene; long-term disturbances.

**Received** 31 August 2018; accepted 4 September 2018. Corresponding Editor: Debra P. C. Peters.

† **E-mail:** dilce.rossetti@inpe.br

## Introduction

The Amazonian rainforest is well known as having the world's greatest biodiversity and landscape complexity. The rainforest is linked to global carbon cycling and climate regulations, and this feature of the ecosystem has encouraged floristic inventories and studies to establish biogeographic patterns on a large scale and to understand the functioning and evolution of the forest. As a result, large-scale tree variations were often associated with modern climatic gradients (ter Steege et al. 2006) or soil filtering (ter Steege et al. 1993, Sabatier et al. 1997, Haugaasen and Peres 2006, Pitman et al. 2008). Although lacking consensus and supporting data on a large scale (Guitét et al. 2016), there is agreement that geology is an important factor for other environmental properties, such as soil and climate, which restrict species distribution and diversification in this region (see Baker et al. 2014 for a full review on this topic). In contrast, a consensus on how geology may have interfered in defining the modern distribution of plant communities throughout the Amazonian ecosystem has not yet been achieved. The lithological contrasts between Neogene and Plio-Pleistocene geological formations produced large-scale functional soil units for forest partitioning in Amazonia (Higgins et al. 2011). Landscape disturbances caused by recent geological events have also been proposed to explain the increase in tree diversity following trends of higher soil fertility and smaller seeds of rapid germination (ter Steege et al. 2006). However, high neotropical biodiversity in general has also been related to complex ecological and evolutionary trends due to Neogene tectonics and glacial/interglacial Pleistocene fluctuations (Bush 1994, Rull 2011). A major problem in linking the distribution of plant species to geological processes has generally been the over-simplification of biogeographic models and the misunderstanding of complex geological processes (Guitét et al. 2016).

The design of models based on biological data from several Amazonian areas with an advanced understanding of geological processes seems to be fundamental when analyzing the distribution of the present-day communities of plant species. Improvements in this field have mainly focused on mosaics of open vegetation within the forest matrix (e.g., Fine et al. 2010, Wittmann et al. 2013, Fortunel et al. 2014). Although less emphasized, the Amazonian rainforest is also heterogeneous in composition, structure, and function. A feature of mature and old-growth forests is the hyperdominance of some tree species in contact with forest mosaics in several successional stages. This variation in plant communities was attributed to the global increase in tree growth in response to the increased anthropogenic $CO_2$ atmospheric concentration in the last decades (Baker et al. 2014, Levis et al. 2017). However, several stochastic events of low and localized intensity, such as fires, extreme droughts, blow-downs, storms, or prehistoric anthropogenic land clearings, were also claimed as the cause of large-scale changes in tropical forests (Nelson et al. 1994, Espírito-Santo et al. 2010, Newbery et al. 2013, Tanner et al. 2014). For instance, African rainforests showed large-scale changes even with small fluctuations in intensity or duration of the dry season (Malhi et al. 2013). A recent publication has also related large-scale changes in the Amazonian rainforest to seasonal variations (Zemp et al. 2017). A growing perception, however, has been that variations within present-day tropical forests were imprinted by long-term (i.e., secular to millennial scale) environmental changes (Patton et al. 2000, Vlam et al. 2017, and references contained therein). Thus, identifying the timing and mode of forest establishment and development is critical to examine the origin of the forest's present-day diversity and understand its functionality.

Large-scale tree mortality and regeneration over a decadal timescale can be detected by forest monitoring, but many of these processes in modern tropical forests are inherited from past disturbances at a centennial (Burslem et al. 2000, Baker et al. 2005), millennial (Daïnou et al. 2010, Lebamba et al. 2012), or perhaps an even longer timescale. Some studies on tree rings from non-Amazonian areas have provided information on long-term (i.e., centennial) disturbances in tropical forests (Baker et al. 2005, Middendorp et al. 2013, Nock et al. 2016, Vlam et al. 2017). Untangling the long-term history of forest disturbances in Amazonia requires floristic and geological data, which can be obtained through the analysis of the sedimentary record. While this is a long-term research that needs to integrate efforts of

botanists and geologists, advancing this field can help researchers better understand the processes of tropical forest development and the origin of the high heterogeneity in tree communities in diverse Amazonian ecosystems.

We investigated tree forests in an extensive area of the middle Madeira River in the southwestern Amazonian plains (Fig. 1), where high sedimentary dynamics induced by tectonic reactivations in the Late Pleistocene–Holocene period was previously documented (e.g., Rossetti et al. 2014). The aim was to examine the effects of geological disturbances in the past and present-day forest composition and structuring, and to link these events to climatic patterns. A previously established geological framework (Fig. 1A) was analyzed in light of new sedimentological and chronological data, the latter obtained by radiocarbon and optically stimulated luminescence (OSL) dating. Floristic inventories led to the characterization of present-day forest types and compositions. C/N and $\delta^{13}C$ analyses of sedimentary organic matter allowed the determination of the time of the last colonization of trees across the studied terrains. The combination of these procedures provided a robust database to examine whether the heterogeneous pattern of the present-day forest is related to past environmental disturbances within the period of a millennial scale or more, an issue that has not yet been investigated (Clark et al. 2010). This may also facilitate the evaluation of links among vegetation patterns, geological processes, and climatic history along the Late Pleistocene–Holocene. Capturing long-term forest disturbances in this area of still undisturbed tree canopies has the potential to contribute to advancing understanding of the potential mechanisms that determine trends in tree growth and forest diversity in many tropical regions.

## GEOLOGICAL FRAMEWORK

We investigated geological and floristic data from an area marginal to the Madeira River in the lowlands of southwestern Amazonia in detail (Fig. 1A, B). This tropical region presents an average annual temperature of 28°C and an average precipitation of 2500–3000 mm/year. The vegetation mainly consists of ombrophylous forest, with local spots of open (savanna-like) vegetation (Radambrasil 1978), the latter being a topic of an ongoing work to be presented elsewhere. The topography is essentially low and flat, with altitudes generally less than 100 m.

The study area is located in the intracratonic basin of Solimões (Fig. 1A), which was established on Precambrian rocks of the Amazonian Craton mainly during the Paleozoic period (Tassinari and Macambira 1999). This basin evolved into a foreland structure from the Cretaceous to the Cenozoic due to the Andean uplifting. Its sedimentary fill is up to 3.8 km thick, but on the surface, it consists of deposits mapped as the Içá Formation of an estimated Plio–Pleistocene age (cf. Maia et al. 1977). In addition, Pleistocene–Holocene to modern alluvial sediments are recorded over a wide area, particularly in the Madeira River basin. The deposits in this region occur on three geomorphological units (T1–T3; Fig. 1B) that record the sedimentary history of fluvial systems during the late Quaternary (Rossetti et al. 2014). T1 is the highest terrain that stands at elevations ranging from 100 to 65 m. Despite the mapping of these deposits as part of the Içá Formation, dating of sediment samples from this plateau recorded only Late Pleistocene OSL ages between 65.4 ± 16.9 and 346.6 ± 48.6 ky (Rossetti et al. 2015), and the $^{14}C$ ages before 43,500 and 31,696–32,913 cal yr BP (Rossetti et al. 2014). T2 is a fluvial terrace recorded on the left bank of the Madeira River at elevations of 85–50 m. This terrace is composed of fluvial deposits with $^{14}C$ ages between 25,338 and 26,056 and 14,129–14,967 cal yr BP. T3 is the youngest terrace formed on both banks of the river at altitudes of 65–45 m and includes deposits younger than 12,881–13,245 cal yr BP.

The history of deposition and erosion of the sedimentary terrains marginal to the Madeira River was related to neotectonic reactivations of the Madre de Dios-Itacoatiara Transcurrent Fault Zone (Souza–Filho et al. 1999, Rossetti et al. 2014). According to these authors, this structure, which parallels the modern Madeira River, also controlled its course in the past. This is shown, for instance, by the large-scale avulsion of this river to the northwest of the study area, recorded by a segment almost 200 km long from a paleovalley approximately 20 km west of the modern river (Hayakawa et al. 2010). In addition, a
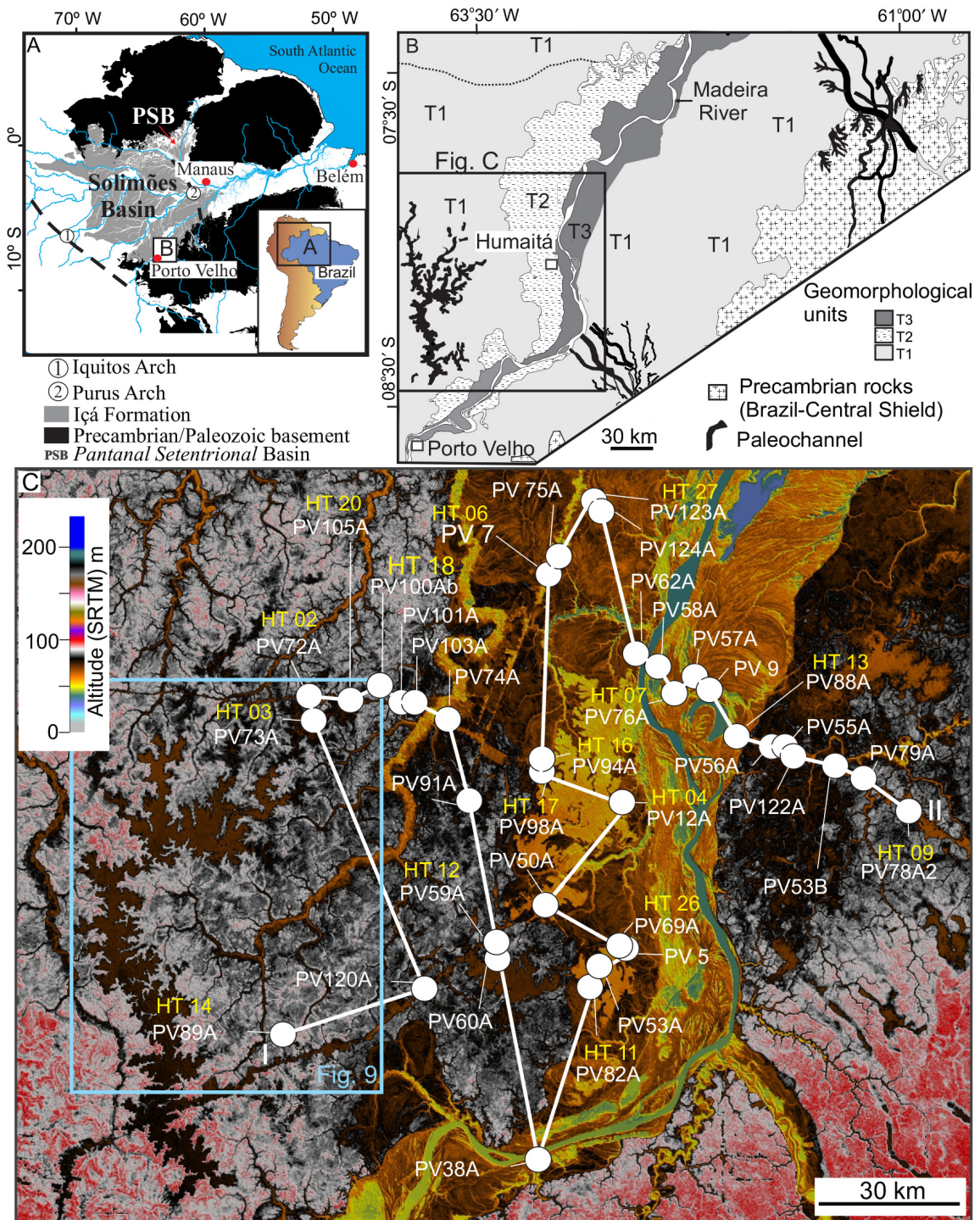
Fig. 1. Location map. (A, B) Location of the study area in the Solimões Basin of lowland Amazonia and simplified geological context (modified from Rossetti et al. 2014). (C) DEM-SRTM with location of the studied transect (I–II) along the valley of the Madeira River, with indication of all geological sections (PV) and floristic inventories (HT).

paleodrainage network in the western sector of the study area was related to the inversion of previous tributaries of the Madeira River due to tectonic tilting (Bertani et al. 2015). A profusion of other documented fluvial paleolandforms on this region also evidences tectonic control (Hayakawa and Rossetti 2015), although a genesis linked to climate changes has also been proposed (Latrubesse 2002).

## Materials and Methods

The study in southwestern Amazonia was based on a transect across the Madeira River (Fig. 1C), which was chosen for its location in an area with extensive and still pristine forest cover. Here, we define as pristine those forests with no detectable evidence of extensive deforestation, logging, fire, or other anthropogenic activities that may have influenced the structure and composition of vegetation over the past few centuries. It is not possible to be sure if the forests studied here were managed by pre-Columbian Amerindian populations (sensu Levis et al. 2017), since the disturbances caused by this management are difficult to detect at the present times. However, stands with high density (>10 adult individuals/ha) of Brazil nut trees (*Bertholletia excelsa*, Lecythidaceae) were excluded from the study due to the putative anthropic origin of these forests in the Rio Madeira region (Scoles and Gribel 2011, 2015) and in the Amazon as a whole. In addition to the pristine forest, the area of the Madeira River was chosen due to the availability of detailed paleoenvironmental reconstruction in the latest geological history based on previous sedimentological and chronological studies, and expressive geological disturbances related to the high fluvial dynamics of the Madeira River by tectonic reactivations. This set of features rendered this area as highly suitable to test whether and how millennial-scale sedimentary events affected the establishment and development of present-day forest tree communities.

The geological framework and detailed reconstructions of fluvial terraces of the Madeira River were presented in previous publications (Rossetti et al. 2014, Bertani et al. 2015; Fig. 1B). Additional geological data-based outcrops (river bank, road cut) and cores were collected at individual sites to complete the existing interpretation of the geological history. The cores were collected using an RKS percussion drilling system, model COBRA mk1 (Eijkelkamp Agrisearch Equipment, Giesbeek, The Netherlands), which provided 5 cm diameter continuous cores at depths up to 15 m. The new data consisted of boreholes acquired with a manual soil sampling auger with a 20-cm sampler. Descriptions of facies included characteristics such as lithology, texture, sedimentary structure, and the type of facies contact, which were recorded in measured lithostratigraphic sections. A total of 37 sections were used to improve the geological knowledge and provide information along a transect that recorded different geological settings of the study area on both banks of the Madeira River (Figs. 1C, 2, and 3). While 30 sections were acquired exclusively for this work, we also added seven sections already reported in a previous publication (Rossetti et al. 2015) to complete the geological view along the transect studied. Among all sections, 18 recorded the geomorphological unit T1, of which 12 were on the western bank of the Madeira River and six were on the eastern bank of this river. Units T2 and T3 were represented by 12 and 7 sections, respectively.

In addition to 23 ages published by Rossetti et al. (2014), we dated an additional 48 sediment samples (Fig. 3, Tables 1–3), which helped us to improve the chronological framework using both $^{14}$C and OSL techniques. The $^{14}$C ages were obtained for 23 samples (Table 1) by an accelerator mass spectrometer (AMS) at Beta Analytic Radiocarbon Dating Laboratory, Florida, USA. Sampling did not follow regular spacing but depended on the availability of fresh, organic-rich muddy sediments. Acceptance was defined as the total laboratory error known to be within 2-sigma. The equipment used in these analyses was the Thermo Delta-Plus isotope ratio mass spectrometer ($\delta^{13}$C precision of $\pm 0.3\permil$) and the single-stage 250-kV NEC particle accelerator (AMS precision of $\pm 0.001$–$0.004$ fractions modern). The radiocarbon ages are reported in years before AD 1950 (yr BP), normalized to $\delta^{13}$C of $-25\permil$ VPDB and in cal yr BP according to SHCal13 (Reimer et al. 2013). The software CALIB Radiocarbon Calibration version 7.1 html (Stuiver et al., 2018) was used for age calibration. The OSL ages were obtained for 25 samples (Fig. 3, Tables 2 and 3) in the Laboratory of
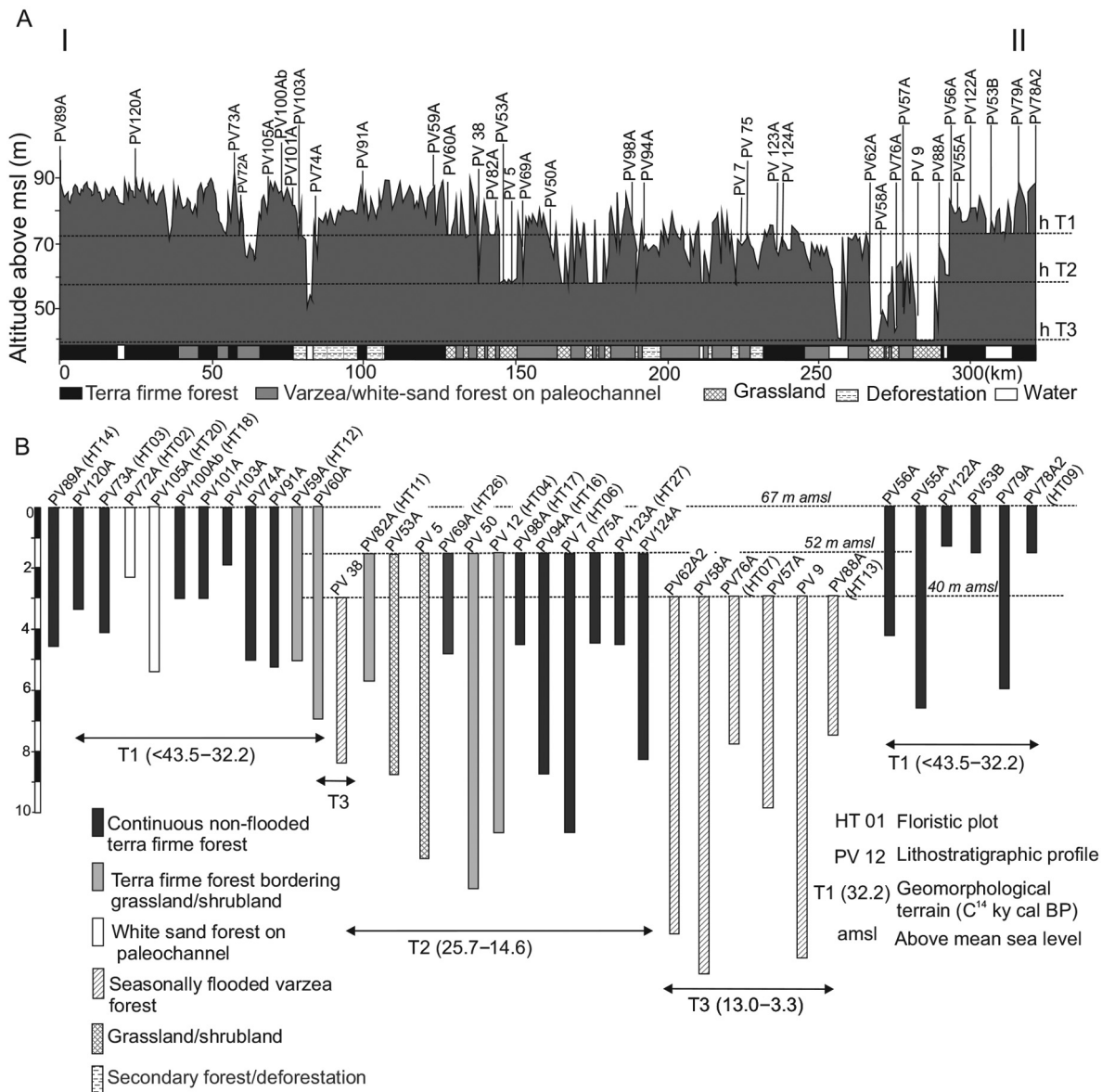
Fig. 2. Topographic framework of the transect I–II (see Fig. 1B for location). (A) Elevations derived from the DEM-SRTM, with indication of the studied geological sections (PV). The horizontal hatched lines indicate the average elevation of individual geomorphological units, discounting the effect of vegetation as interpreted from remote sensing data combined with field observations. (B) Distribution of the geological sections (PV) and floristic plots (HT) along the geomorphological units, with indication of the various types of vegetation cover, interpreted from remote sensing data, Digital Globe and WebGLEarth (webglearth.com) images, and eye views and photographs obtained with a Phantom-3 drone.

Dating and Dosimetry of the Federal University of São Paulo (UNIFESP) using the Risø OSL/TL model DA-20 and DA-15 equipment with blue LEDs, Hoya U-340 filters, and built-in $^{90}$Sr/$^{90}$Y beta sources. We used the single-aliquot regeneration protocol to measure equivalent doses (Murray and Wintle 2003, Duller 2004). The mass fraction of U, Th, K for the calculation of the dose
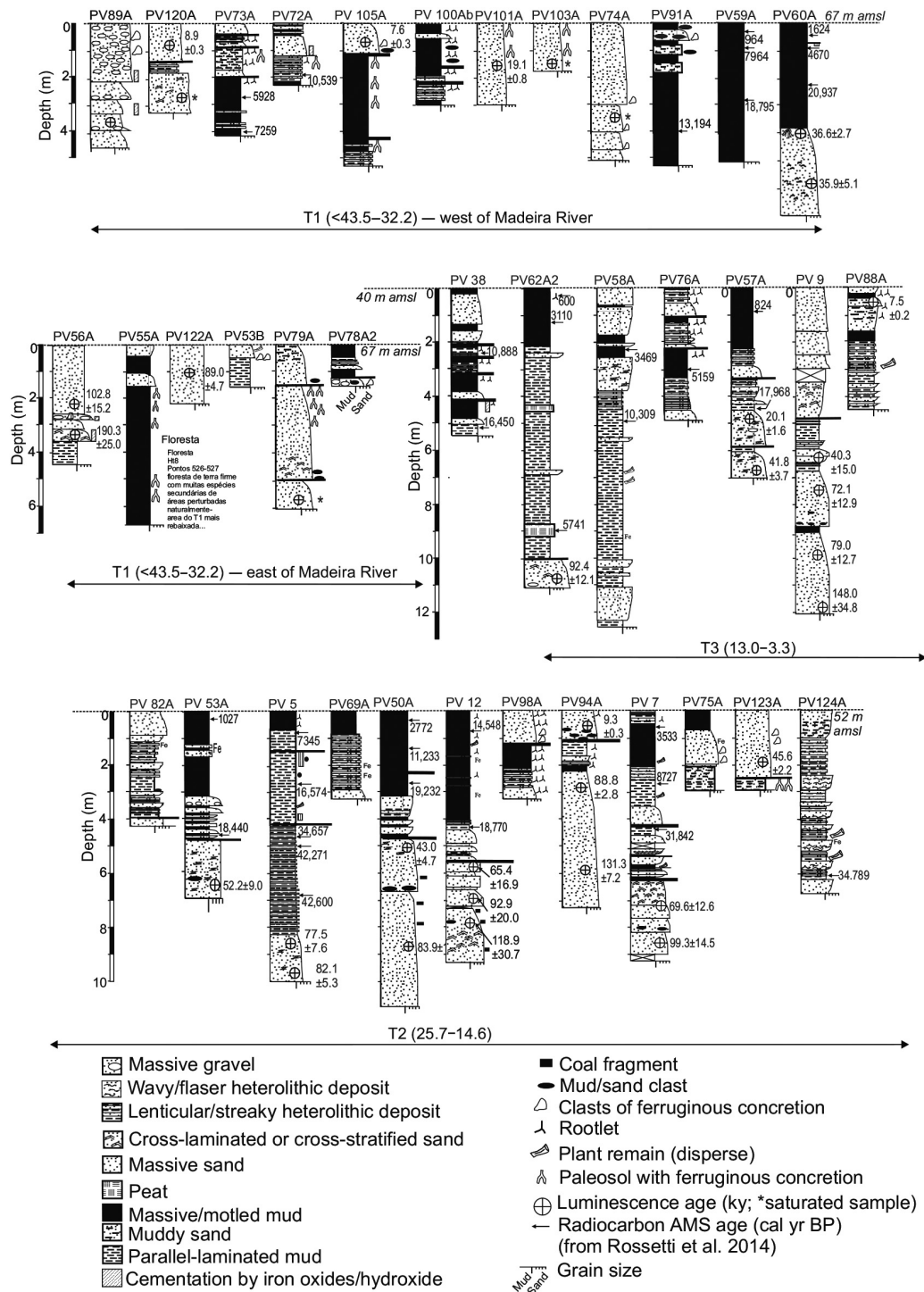
Fig. 3. Geological sections with corresponding chronology based on ^{14}C and OSL dating (see location in Fig. 1 and topographic framework in Fig. 2).

Table 1. AMS $^{14}$C dating of samples derived from sedimentary deposits representative of the three geomorphological units cited in the text.

| Geom unit | Locality/laboratory number | Coordinates | Depth (m) | $^{14}$C yr BP conventional | Cal yr BP 2-sigma calibration-AMS (median probability) |
|---|---|---|---|---|---|
| T2 | PV5 (288718)† | 7°55′26″ S 63°04′60″ W | 0.8 | 6450 (±40) | 7265–7422 (7345) |
| T2 | PV5 (288719)† | 7°55′26″ S 63°04′60″ W | 2.7 | 13,770 (±60) | 16,316–16,863 (16,574) |
| T2 | PV5 (304791)† | 7°55′26″ S 63°04′60″ W | 4.7 | 30,770 (±170) | 34,272–34,999 (34,657) |
| T2 | PV5 (285261)† | 7°55′26″ S 63°04′60″ W | 5.0 | 34,000 (±200) | 41,770–42,768 (42,271) |
| T2 | PV5 (288720)† | 7°55′26″ S 63°04′60″ W | 6.8 | 38,110 (±360) | 42,033–43,168 (42,600) |
| T2 | PV7 (309798)† | 7°18′04″ S 63°10′10″ W | 0.5 | 3350 (±50) | 3446–3641 (3533) |
| T2 | PV7 (304792)† | 7°18′04″ S 63°10′10″ W | 2.7 | 7940 (±40) | 8591–8814 (8727) |
| T2 | PV7 (309799)† | 7°18′04″ S 63°10′10″ W | 4.2 | 28,130 (±140) | 31,431–32,456 (31,842) |
| T2 | PV12 (304797)† | 6°42′28″ S 61°42′28″ W | 0.9 | 12,440 (±50) | 14,129–14,967 (14,548) |
| T2 | PV12 (309801)† | 6°42′28″ S 61°42′28″ W | 4.3 | 15,630 (±60) | 18,626–18,914 (18,770) |
| T3 | PV38 (309812) | 8°13′39″ S 63°12′12″ W | 2.4 | 9650 (±50) | 10,980–10,782 (10,888) |
| T3 | PV38 (309814) | 8°13′39″ S 63°12′12″ W | 5.1 | 13,290 (±50) | 16,610–16,300 (16,450) |
| T2 | PV50A (397678) | 8°49′44″ S 63°10′10″ W | 0.6 | 2700 (±30) | 2742–2844 (2772) |
| T2 | PV50A (406686) | 8°49′44″ S 63°10′10″ W | 1.5 | 9870 (±30) | 11,190–11,275 (11,233) |
| T2 | PV50A (397679) | 8°49′44″ S 63°10′10″ W | 2.9 | 16,000 (±60) | 19,028–19,482 (19,252) |
| T2 | PV53A (397683) | 7°56′27″ S 63°05′02″ W | 0.2 | 1190 (±63) | 963–1094 (1027) |
| T2 | PV53A (397685) | 7°56′27″ S 63°05′02″ W | 4.8 | 15,170 (±50) | 18,287–19,597 (18,440) |
| T3 | PV57 (397688) | 7°28′31″ S 62°56′40″ W | 0.8 | 920 (±30) | 732–922 (824) |
| T3 | PV57 (397687) | 7°28′31″ S 62°56′40″ W | 3.5 | 14,810 (±60) | 17,764–18,167 (17,968) |
| T3 | PV58 (406692) | 7°29′10″ S 63°00′46″ W | 2.2 | 3280 (±30) | 3384–3515 (3459) |
| T3 | PV58 (309814) | 7°29′10″ S 63°00′46″ W | 4.9 | 9200 (±30) | 10,232–10,420 (10,309) |
| T1 | PV59A (406695) | 7°52′16″ S 63°15′26″ W | 0.3 | 1110 (±30) | 924–995 (964) |
| T1 | PV59A (406696) | 7°52′16″ S 63°15′26″ W | 0.9 | 7180 (±30) | 7871–7895 (7964) |
| T1 | PV59A (397693) | 7°52′16″ S 63°15′26″ W | 2.8 | 15,580 (±60) | 18,645–18,926 (18,795) |
| T1 | PV60A (397695) | 7°54′30″ S 63°14′54″ W | 0.4 | 1750 (±30) | 1469–1748 (1624) |
| T1 | PV60A (406698) | 7°54′30″ S 63°14′54″ W | 0.8 | 4170 (±30) | 4529–4729 (4670) |
| T1 | PV60A (397696) | 7°54′30″ S 63°14′54″ W | 2.2 | 17,400 (±60) | 20,700–21,182 (20,937) |
| T3 | PV62A2 (397702)‡ | 7°26′15″ S 63°01′11″ W | 0.2 | 630 (±30) | 552–613 (600) |
| T3 | PV62A2 (397703)‡ | 7°26′15″ S 63°01′11″ W | 1.3 | 2950 (±30) | 3001–3183 (3110) |
| T3 | PV62A2 (397701)‡ | 7°26′15″ S 63°01′11″ W | 9.0 | 5010 (±30) | 5655–5766 (5741) |
| T1 | PV72A2 (476312) | 7°29′50″ S 63°32′54″ W | 1.9 | 9370 (±30) | 10,418–10,607 (10,539) |
| T1 | PV73A (476313) | 7°30′39″ S 63°32′51″ W | 2.7 | 5210 (±30) | 5886–5995 (5928) |
| T1 | PV73A (476314) | 7°30′39″ S 63°32′51″ W | 4.0 | 6370 (±30) | 7166–7325 (7259) |
| T3 | PV76A (476315) | 7°29′04″ S 62°57′48″ W | 3.0 | 4550 (±30) | 5053v5189 (5159) |
| T1 | PV91A (476317) | 7°39′42″ S 63°17′23″ W | 4.0 | 11,350 (±30) | 13,111–13,281 (13,194) |
| T2 | PV124A (476327) | 7°11′50″ S 63°06′49″ W | 6.3 | 30,880 (±160) | 34,452–35,138 (34,789) |

*Note:* All samples are derived from organic sedimentary deposits.

† Age from Rossetti et al. (2014).

‡ Age from Rossetti et al. (2015).

rates was determined by instrumental neutron activation analysis (INAA) with a Germanium (hyperpure) detector, model GX2519 from Canberra, with a resolution of 1.90 keV at the 1332.49 keV γ-peak of $^{60}$Co. The samples were irradiated in the swimming pool research reactor IEA-R1 of the Nuclear and Energy Research Institute, IPEN-CNEN/SP, at a thermal neutron flux of $1.2 \times 1012$ cm$^{-2} \cdot$ s$^{-1}$ for 8 h. Spectra were collected with a Canberra S-100 multi-channel analyzer with 8196 channels. The Standard Reference Material NIST-SRM1633b was used as standard for analysis and the IAEA-Soil-7 for the analytical quality control. The software Genie-2000 NAA Processing Procedure was used to analyze the gamma-ray spectra. The daughter nuclides were also calculated with an efficiency calibration based on the ISOCS (In Situ Object Counting System) for the used HPGe detector. The total error of dose rates and ages was

Table 2. Summary of radioisotope concentrations in samples dated by optically stimulated luminescence.

| Sample | Coordinate lat/long | Depth (m) | U ppm | Th ppm | K % | Water (%) |
|--------|---------------------|-----------|-------|--------|-----|-----------|
| PV5 | 7°55′26″ S (63°04′60″ W) | 8.6 | 4.49 ± 0.07 | 13.20 ± 0.15 | 1.86 ± 0.01 | 28 |
| PV5 | 7°55′26″ S (63°04′60″ W) | 9.7 | 5.00 ± 0.08 | 17.57 ± 0.17 | 2.15 ± 0.02 | 29 |
| PV7† | 7°18′04″ S (63°10′10″ W) | 7.2 | 3.17 ± 0.58 | 9.16 ± 0.55 | 1.19 ± 0.19 | 43 |
| PV7† | 7°18′04″ S (63°10′10″ W) | 8.4 | 1.67 ± 0.56 | 7.53 ± 0.53 | 1.12 ± 0.26 | 45 |
| PV9† | 7°29′31″ S (62°55′43″ W) | 6.3 | 3.65 ± 0.53 | 9.30 ± 0.82 | 1.15 ± 0.04 | 32 |
| PV9† | 7°29′31″ S (62°55′43″ W) | 7.3 | 1.88 ± 0.39 | 8.25 ± 0.50 | 1.10 ± 0.15 | 43 |
| PV9† | 7°29′31″ S (62°55′43″ W) | 9.7 | 1.73 ± 0.40 | 7.48 ± 0.47 | 1.22 ± 0.19 | 43 |
| PV9† | 7°29′31″ S (62°55′43″ W) | 12.3 | 0.64 ± 0.31 | 2.92 ± 0.38 | 0.56 ± 0.12 | 43 |
| PV12† | 7°37′38″ S (63°04′87″ W) | 5.6 | 3.20 ± 0.56 | 9.75 ± 0.60 | 1.55 ± 0.53 | 27 |
| PV12† | 7°37′38″ S (63°04′87″ W) | 6.8 | 1.84 ± 0.42 | 7.05 ± 0.43 | 1.1 ± 0.44 | 30 |
| PV12† | 7°37′38″ S (63°04′87″ W) | 7.7 | 1.95 ± 0.50 | 9.96 ± 0.61 | 1.16 ± 0.68 | 40 |
| PV50A | 8°49′44″ S (63°10′10″ W) | 4.8 | 3.11 ± 0.41 | 10.12 ± 0.55 | 1.45 ± 0.30 | 22 |
| PV50A | 8°49′44″ S (63°10′10″ W) | 8.7 | 2.95 ± 0.42 | 12.2 ± 0.65 | 1.21 ± 0.72 | 30 |
| PV53A | 7°56′27″ S (63°05′02″ W) | 4.9 | 2.88 ± 0.36 | 10.24 ± 0.38 | 1.23 ± 0.52 | 17 |
| PV56A† | 7°33′40″ S (62°50′09″ W) | 2.2 | 2.48 ± 0.00 | 13.06 ± 0.00 | 0.51 ± 0.03 | 4 |
| PV56A† | 7°33′40″ S (62°50′09″ W) | 3.4 | 1.19 ± 0.00 | 5.71 ± 0.00 | 0.26 ± 0.02 | 10 |
| PV57A | 7°28′31″ S(62°56′40″ W) | 4.8 | 3.55 ± 0.51 | 9.10 ± 0.72 | 1.16 ± 0.20 | 19 |
| PV57A | 7°28′31″ S (62°56′40″ W) | 6.9 | 1.90 ± 0.29 | 8.63 ± 0.47 | 1.14 ± 0.17 | 25 |
| PV60A | 7°54′30″ S (63°14′54″ W) | 4.3 | 3.08 ± 0.36 | 12.03 ± 0.61 | 1.36 ± 0.15 | 28 |
| PV60A | 7°54′30″ S (63°14′54″ W) | 5.7 | 3.22 ± 0.45 | 10.04 ± 0.55 | 1.65 ± 0.51 | 30 |
| PV62A2 | 7°26′15″ S (63°01′11″ W) | 10.8 | 2.34 ± 0.42 | 11.2 ± 0.50 | 0.61 ± 0.03 | 13 |
| PV74A | 7°31′27″ S (63°20′43″ W) | 6.0 | – | – | – | – |
| PV79A2 | 7°37′54″ S (62°39′49″ W) | 6.0 | – | – | – | – |
| PV88A | 7°32′55″ S (62°52′38″ W) | 0.5 | 1.55 ± 0.07 | 5.99 ± 0.30 | 0.15 ± 0.01 | 9 |
| PV94A1 | 7°35′34″ S (63°11′23″ W) | 0.5 | 1.75 ± 0.07 | 6.46 ± 0.38 | 0.10 ± 0.01 | 7 |
| PV94A3 | 7°35′34″ S (63°11′23″ W) | 3.0 | 1.80 ± 0.07 | 6.65 ± 0.39 | 0.11 ± 0.01 | 7 |
| PV94A2 | 7°35′34″ S (63°11′23″ W) | 5.8 | 1.89 ± 0.07 | 7.14 ± 0.42 | 0.17 ± 0.01 | 8 |
| PV101A1 | 7°30′04″ S (63°24′55″ W) | 1.8 | 2.73 ± 0.07 | 14.04 ± 0.70 | 0.20 ± 0.01 | 10 |
| PV103A1 | 7°30′18″ S (63°22′17″ W) | 1.7 | – | – | – | – |
| PV105A1 | 7°30′02″ S (63°28′53″ W) | 0.7 | 3.90 ± 0.07 | 14.08 ± 0.61 | 0.08 ± 0.01 | 8 |
| PV120A1 | 7°57′18″ S (63°21′41″ W) | 0.9 | 1.81 ± 0.07 | 9.35 ± 0.43 | 0.08 ± 0.01 | 8 |
| PV120A3 | 7°57′18″ S (63°21′41″ W) | 3.0 | – | – | – | – |
| PV122A1 | 7°33′43″ S (62°48′45″ W) | 1.0 | 2.10 ± 0.07 | 7.14 ± 0.44 | 0.05 ± 0.01 | 8 |
| PV123A1 | 7°17′14″ S (63°09′48″ W) | 2.5 | 2.05 ± 0.07 | 9.31 ± 0.40 | 0.10 ± 0.01 | 7 |
| PV124A1 | 7°11′50″ S (63°06′49″ W) | 5.7 | – | – | – | – |

*Note:* En dash indicates below detection.
† Age from Rossetti et al. (2015).

calculated according to the Gaussian law of error propagation. The number of aliquots per sample ranged from 9 to 16, with exponential or linear–exponential growth functions used to describe dose–response curves. The central (Galbraith and Roberts 2012) or finite mixture (Galbraith and Green 1990) age models were used when the equivalent dose (De) dispersion values were lower or higher than 20%, respectively. The values of De were calculated using the numerical software package statistical numOSL (Peng et al. 2013). We only used aliquots with the recycling test <10% and recovery test <5%.

We selected 12 geological sections (Figs. 4–6) to perform analyses of total organic carbon, total nitrogen, and $\delta^{13}C$ to reconstruct changes in vegetation patterns before the establishment of the present-day forest. Among these sections, five were from unit T1, four were from unit T2, and three were from unit T3. Soil degradation can enrich $^{13}C$ (e.g., Chikaraishi and Naraoka 2006, Garcin et al. 2014, Schwab et al. 2015), but the $\delta^{13}C$ values in the soil are within the range of the values of present-day plants (Garcin et al. 2014). For this reason, this proxy has been used in paleoclimatic reconstructions (Meyers 1997, Cloern et al. 2002,

Table 3. Optically stimulated luminescence dated samples with corresponding depths, equivalent doses (De), total annual dose rate (AD), aliquot number (N), and ages.

| Sample | Depth (m) | De (Gy) | AD (Gy/ky) | N | Age (ky) |
|---|---|---|---|---|---|
| PV5 | 8.6 | 261 ± 25 | 3.37 ± 0.69 | 16 | 77.5 ± 7.6 |
| PV5 | 9.7 | 284 ± 15 | 3.46 ± 0.13 | 16 | 82.1 ± 5.3 |
| PV7 | 7.2 | 124 ± 20 | 1.78 ± 0.14 | 16 | 69.6 ± 12.6 |
| PV7 | 8.4 | 138 ± 12 | 1.39 ± 0.16 | 16 | 99.0 ± 14.5 |
| PV9† | 6.3 | 81 ± 20 | 2.02 ± 0.11 | 12 | 40.3 ± 15.0 |
| PV9† | 7.3 | 107 ± 17 | 1.49 ± 0.11 | 16 | 72.1 ± 12.9 |
| PV9† | 9.7 | 116 ± 16 | 1.48 ± 0.12 | 16 | 79.0 ± 12.7 |
| PV9† | 12.3 | 94 ± 19 | 0.63 ± 0.08 | 16 | 148 ± 34.8 |
| PV12† | 5.6 | 154 ± 3 | 2.36 ± 0.35 | 16 | 65.4 ± 16.9 |
| PV12† | 6.8 | 146 ± 2 | 1.57 ± 0.28 | 11 | 92.9 ± 20.2 |
| PV12† | 7.7 | 195 ± 2 | 1.64 ± 0.39 | 09 | 118.9 ± 30.7 |
| PV50A | 4.8 | 123 ± 8 | 2.86 ± 0.25 | 16 | 43.0 ± 4.7 |
| PV50A | 8.7 | 221 ± 10 | 2.66 ± 0.57 | 16 | 83.9 ± 18.3 |
| PV53A | 4.9 | 105 ± 8 | 2.01 ± 0.31 | 16 | 52.2 ± 9.0 |
| PV56A† | 2.2 | 200 ± 26 | 1.95 ± 0.14 | 11 | 102.8 ± 15.2 |
| PV56A† | 3.4 | 200 ± 22 | 1.05 ± 0.07 | 11 | 190.2 ± 25.4 |
| PV57A | 4.8 | 53 ± 2 | 2.64 ± 0.19 | 16 | 20.1 ± 1.6 |
| PV57A | 6.9 | 90 ± 5 | 2.15 ± 0.15 | 16 | 41.8 ± 3.7 |
| PV60A | 4.3 | 105 ± 6 | 2.87 ± 0.14 | 16 | 36.6 ± 2.7 |
| PV60A | 5.7 | 108 ± 5 | 3.01 ± 0.41 | 16 | 35.9 ± 5.1 |
| PV62A2† | 10.8 | 185 ± 19 | 2.00 ± 0.16 | 09 | 92.4 ± 12.0 |
| PV74A | 6.0 | – | – | – | ‡ |
| PV79A2 | 6.0 | – | – | – | ‡ |
| PV88A | 0.5 | 12.6 ± 0.3 | 1.03 ± 0.25 | 08 | 7.5 ± 0.2 |
| PV94A1 | 0.5 | 10.7 ± 0.2 | 1.15 ± 0.27 | 11 | 9.3 ± 0.3 |
| PV94A3 | 3.0 | 109 ± 2 | 1.23 ± 0.30 | 15 | 88.8 ± 32.8 |
| PV94A2 | 5.8 | 125 ± 6 | 0.95 ± 0.28 | 12 | 131.3 ± 7.2 |
| PV101A1 | 1.8 | 37.5 ± 1.0 | 1.96 ± 0.47 | 16 | 19.1 ± 0.8 |
| PV103A1 | 1.7 | – | – | – | ‡ |
| PV105A1 | 0.7 | 16.3 ± 0.3 | 2.14 ± 0.65 | 14 | 7.6 ± 0.80.3 |
| PV120A1 | 0.9 | 13.2 ± 0.3 | 1.49 ± 0.34 | 17 | 8.9 ± 0.3 |
| PV120A3 | 3.0 | – | – | – | ‡ |
| PV122A1 | 1.0 | 125 ± 6 | 1.40 ± 0.30 | 11 | 89.0 ± 4.7 |
| PV123A1 | 2.5 | 75 ± 3 | 1.64 ± 0.36 | 09 | 45.6 ± 2.2 |
| PV124A1 | 5.7 | – | – | – | ‡ |

*Note:* N is number of measured aliquot. En dash indicates below detection.
† Age from Rossetti et al. (2015).
‡ Saturated sample.

Ogrinc et al. 2005), with values between −33.0‰ and −23.0‰, and between −15.0‰ and −9.0‰ being related to $C_3$ and $C_4$ terrestrial plants, respectively (Deines 1980). Since the $\delta^{13}C$ values of terrestrial plants may overlap with those of aquatic plants, the isotopic ratio should be used with C/N to discriminate freshwater phytoplankton (C/N = 4.0 to 10.0; Meyers 1997) from land plants (C/N ≥ 12.0; e.g., Cloern et al. 2002, Wilson et al. 2005). These proxies were applied in sections with chronologically similar sedimentary records on the studied plateaus in an attempt to detect

and compare the time for the establishment of modern forests. Samples, generally collected at intervals of 20 cm, were prepared following standard procedures in the Iso-Analytical Laboratory of England. The reference material used during the $\delta^{13}C$ analysis of acid-washed samples was IA-R001 (wheat flour, $\delta^{13}C_{V-PDB}$ = of −26.43‰). The results were expressed as percentage dry weight (total C and N) and as $\delta^{13}C$ over the VPDB standard using conventional δ (‰) notations.

We inventoried 16 forest plots (Figs. 1C and 2B), which covered a total of 4.5 ha, with each
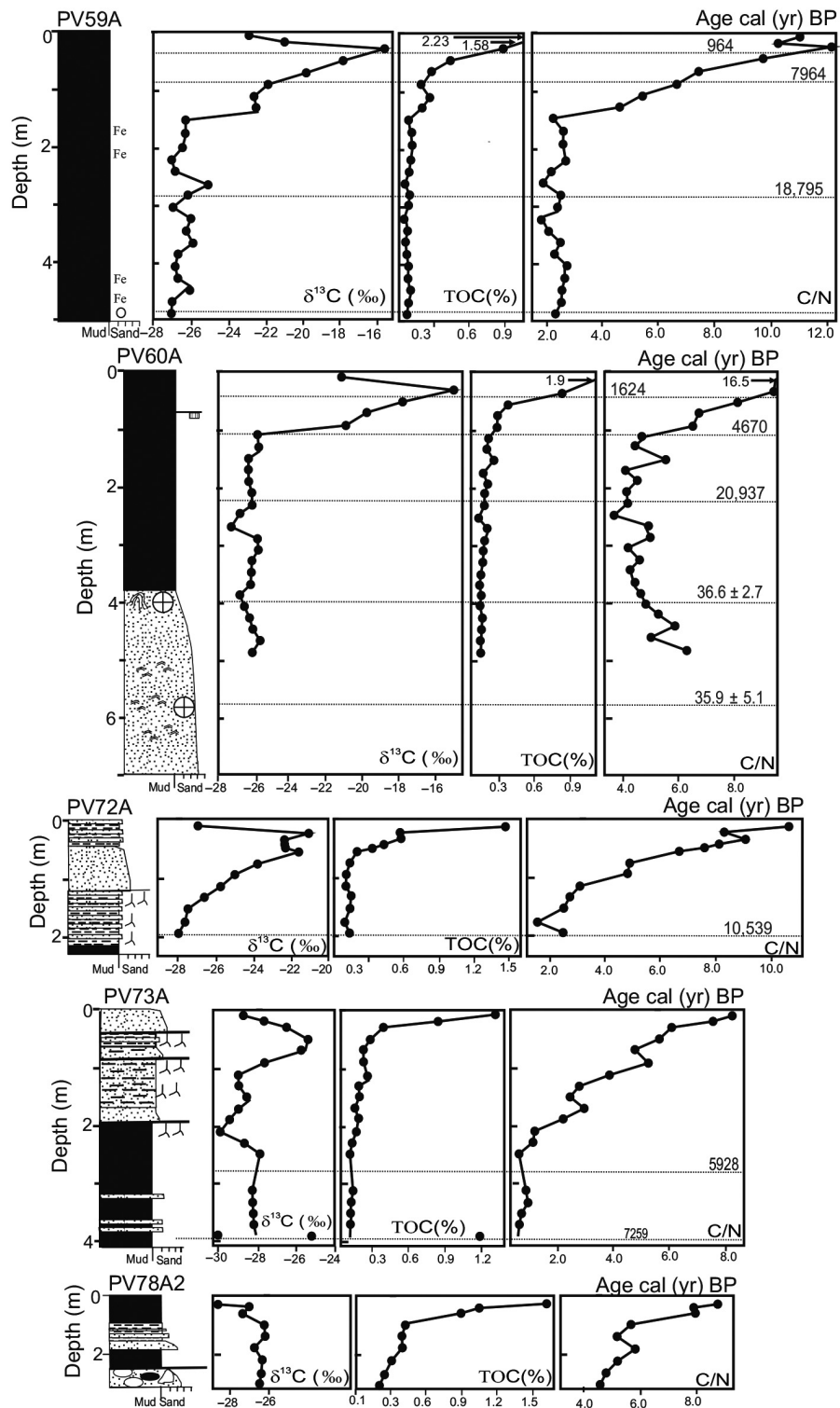
Fig. 4. $\delta^{13}$C, TOC, and C/N data from geological sections located in the T1 unit (see Fig. 1 for location).

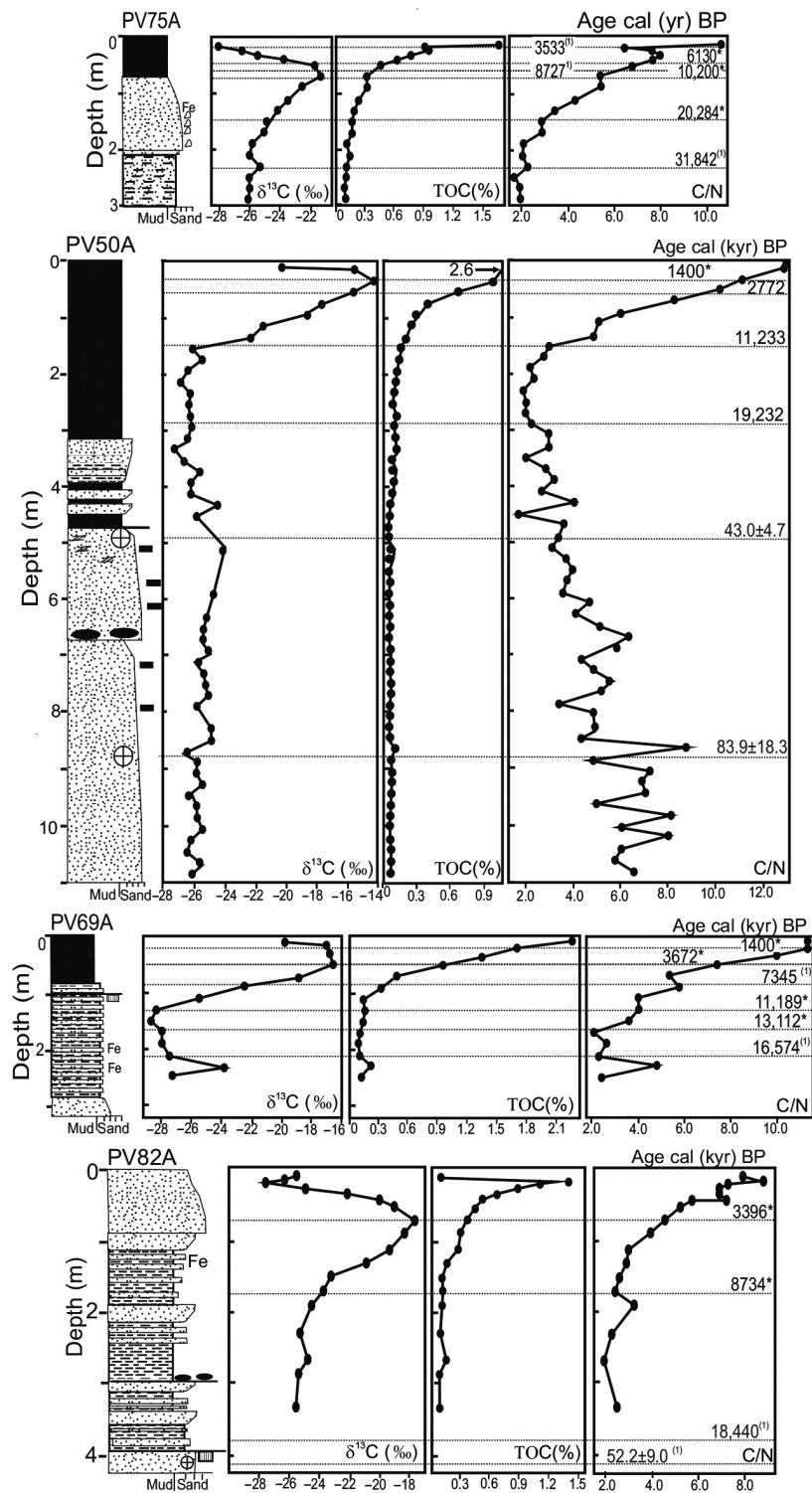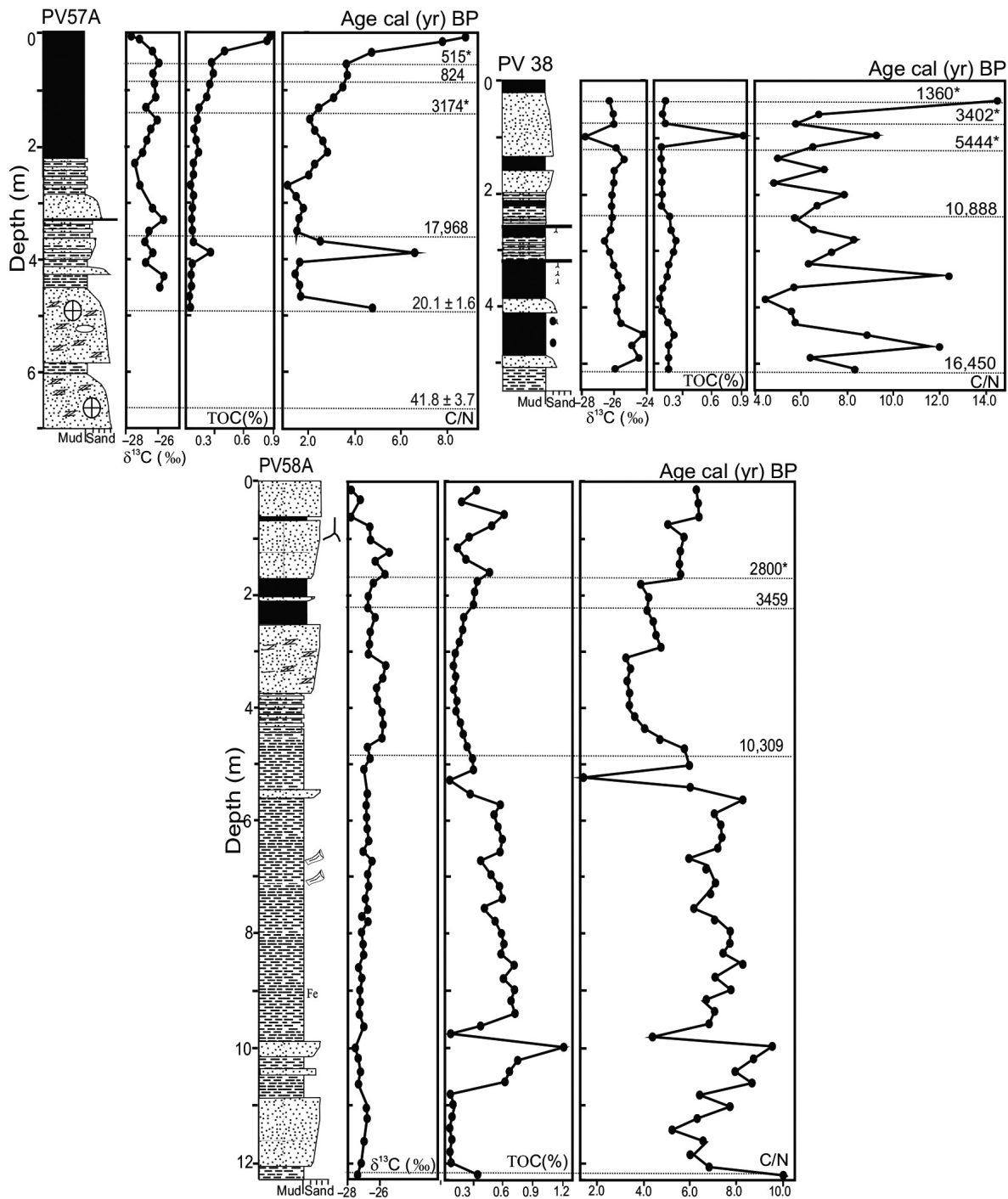Fig. 5. $\delta^{13}$C, TOC, and C/N data from geological sections located in the T2 unit (see Fig. 1 for location).

Fig. 6. $\delta^{13}$C, TOC, and C/N data from geological sections located in the T3 unit (see Fig. 1 for location).

plot varying in size from 0.2 e 0.5 ha. All trees had a diameter at breast height ≥30 cm, and their crowns reached the canopy or sub-canopy. For the comparison of the plots, the abundance and basal area were standardized to 1 ha (individuals/ha and m$^2$/ha, respectively). Each plot was categorized according to forest types (cf. IBGE 2012) and positions in the geomorphological

units T1–T3 (cf. Rossetti et al. 2014) as follows: non-flooded terra firme forest in units T1 (HT03, HT09, HT14, HT18) and T2 (HT04, HT06, HT11, HT16, HT17, HT26, HT27); white-sand campinarana forest on paleochannels in unit T1 (HT02, HT12, HT20); and seasonally flooded varzea forest in unit T3 (HT07, HT13). Terra firme forests were further classified as continuous (HT03, HT06, HT14, HT09, HT16, HT17, HT18, HT27) and ecotonal (HT04, HT11, HT26). Ecotonal forests consist of border forests in contact with regional savannas (Gottsberger and Morawetz 1986), the latter being complex formations to be dealt with more detail in a separate publication. Relative abundance (i.e., the proportion of individuals of each species per plot) was processed by cluster analysis to establish the floristic relationship among the inventoried plots. The UPGMA (unweighted pair-group method using arithmetic averages) clustering was applied with the Bray-Curtis similarity index (Bray and Curtis 1957), and each binding was tested with a 1000-bootstrap resampling. The percentages of replicates that each dendrogram node supports were provided. To ordinate and graphically express the floristic relationship among the plots, we performed the NMDS (non-metric multidimensional scaling; Krustal and Wish 1978) analysis using the basal area ($m^2$/ha) for each species per plot as the abundance relative to the measure. The data were transformed by square root before analysis to avoid overweight of the highly frequent species (Clarke and Green 1988, Clarke 1993). Trees were preliminarily identified in the field with the help of experienced botanists, and the samples were classified at the lowest possible taxonomic level in comparison with reference specimens deposited in the herbarium of the National Institute of Amazonian Research and virtual collections (such as: http://reflora.jbrj.gov.br/reflora/PrincipalUC/PrincipalUC.do?lingua=en).

We used the original (30m-resoluiton) digital elevation model (DEM) from the Shuttle Radar Topography Mission (SRTM) for topographic characterization (downloaded from https://www2.jpl.nasa.gov/srtm/). In addition, high-resolution optical images from Digital Globe and WebGLEarth (webglearth.com) as well as views and photographs taken with a Phantom-3 drone completed our analysis of the forest structure.

## RESULTS

### Sedimentological characteristics and depositional environments

The facies analysis revealed that the three geomorphological units consist of siliciclastic lithologies that vary in grain size from mud to sand, and locally gravel (Fig. 3). Massive and cross-stratified gravels and sands were formed by high-energy flows within channels as evidenced by fining-upward successions <5 m thick and based on sharp erosional surfaces locally with intraformational pebbles. The channelized deposits were amalgamated or interbedded with low-energy floodplain strata. The latter consisted of massive or parallel-laminated mud intergraded with various proportions of sand and mud as streaky, lenticular, and wavy heterolithic beddings. Floodplain deposits graded upward into coarsening-upward sandy successions <1 m thick were related to crevasse splays of sand overflows into adjacent floodplains at high-channel stages. All these deposits presented different degrees of phytoturbation associated with several local-scale paleosols, which are typical of fluvial environments.

A comparison of the sedimentological characteristics from all geological sections revealed some important differences when the three geomorphological units were compared. Thus, unit T1 showed deposits with a higher degree of induration than the two younger units due to the greater degree of lithification and development of lateritic paleosols, being characterized by incipient ferruginous concretions. Lateritic paleosols were reworked as fragmented concretions within overlying deposits. The iron oxides/hydroxides of these concretions were remobilized and cemented in the surrounding deposits, which further increased the hardness of the unit T1. We found that such processes were less effective in units T2 and T3, which contained softer and usually less oxidized lithologies than T1. In addition, the unit T3 recorded comparatively more frequent and denser floodplain deposits.

Although the studied units were promptly identified by sedimentological, geomorphological, and topographic characteristics presented in Rossetti et al. (2014), their chronology proved to be not so simple due to multiple phases of sediment deposition and erosion, which produced several hiatuses in the sedimentary successions.

In addition, sediment reworking by channels established mainly in units T1 and T2 caused not only erosion, but also added new sediments to their surfaces at different times after the origin of the individual plateaus. As a result, the top of unit T1 had local sedimentary successions to the deposits of units T2 and T3 (Fig. 3) and the top of unit T2 had sediments as young as the age of unit T3. Another important observation was that, although they were deactivated as depositional sites, the paleochannels were still underfilled, in which case they were marked by slightly concave-up morphologies that are still flooded during wet seasons. This is an important information to consider when analyzing the drivers for the present-day forests because communities located within a given geomorphological unit may have several substrates formed at various ages and hydrological conditions.

### Floristic data

The inventory of the 16 forest plots resulted in the record of 306 species, out of which 50 with basal area $\geq 0.59$ m$^2$/ha (Appendix S1; Figs. 7 and 8). The cluster analysis (Fig. 8) based on the relative abundance of species per plot showed three groups, which correspond to the three physiognomies of the forest: campinarana, varzea, and terra firme. The nodes that separate two plots of campinarana forest (HT02 and HT20) and two plots of varzea forest (HT07 and HT13) from forests remaining in the dendrogram were supported by the high proportion of bootstrap resampling (100% and 94%, respectively). The third cluster was formed by twelve plots of terra firme forest, including the HT12 plot located on an inactive channel paleolandform. It was not clear from the analysis how these forest plots were floristically related, since the bootstrap values at the cluster nodes were always low.

The floristic data revealed that the continuous terra firme forests of the units T1 and T2 harbored tree assemblages with some floristic similarity, as shown by their close occurrence in the branches of the cluster dendrogram (Fig. 7). These plots also had the highest diversity (Table 4, Fig. 8A, B) among the sampled forests. Although terra firme forest plots were not distinguished on the basis of their floristic similarity by the clustering analysis, the tree community structure in this forest type varied visibly as the
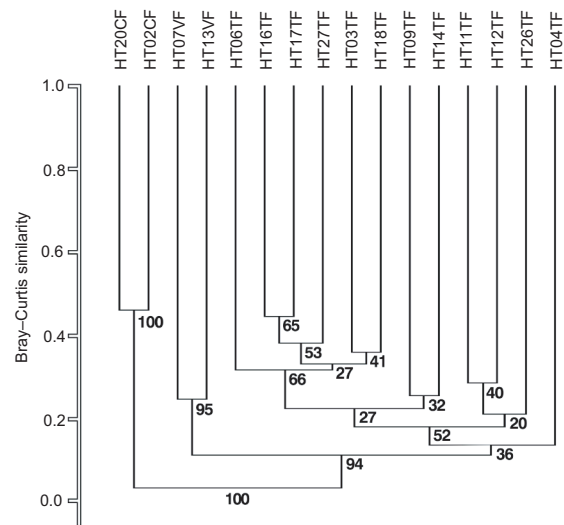


Fig. 7. Dendrogram resulting from the cluster analysis using the Bray-Curtis similarity index of 16 floristic plots inventoried based on the relative abundance of each species per plot. Abbreviations are HT, plot; TF, continuous terra firme forest; EF, ecotonal forest; VZ, varzea forest; CF, campinarana forest on paleochannel.

plots of unit T1 exhibited basal areas larger than those in unit T2 (44.1 and 23.5 m$^2$/ha, respectively; $t$-test, $P = 0.035$; Fig. 8A, C). The continuous forest in unit T1 also recorded taller trees compared to T2 (22.1 and 18.6 m, respectively), although this difference did not have high statistical significance ($t$-test, $P = 0.083$). Two palm species (*Attalea speciosa* Mart and *Euterpe precatoria* Mart, Arenacaceae) were among the five more populous species of these.

*Pouteria guianensis* Aubl. (Sapotaceae) were the more populous trees. The emergent species with the highest basal areas were *Bertholletia excelsa* Bonpl. (Lecythidaceae), *Brosimum parinarioides* Ducke (Moraceae), *Caryocar villosum* (Aubl.) Pers. (Caryocaraceae), *Cariniana micrantha* Ducke (Lecythidaceae), and *Hymenolobium excelsum* Ducke (Fabaceae).

Another difference between units T1 and T2 was that the latter presented a significant proportion of ecotonal forests (i.e., plots HT04, HT11, and HT26) bordering two large savanna vegetation patches. Among these plots, HT11 and HT26 were located in a slope area with ravines that exposed deeper soil layers for tree colonization. The sloping forests were topographically lower
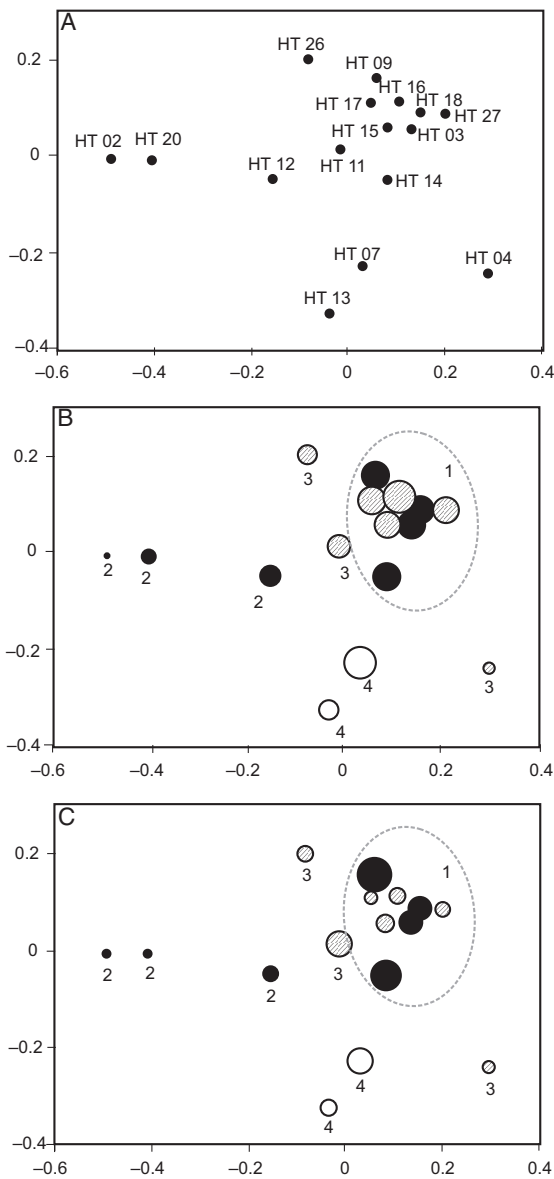
Fig. 8. Non-metric multidimensional scaling (NMDS) ordination showing the floristic relationships of the 16 inventoried forest plots. (A) Identification of each plot. (B, C) Analysis with dot diameters proportional to the Shannon diversity (B) and basal area (C). The black, hatched, and white dots represent plots of units T1, T2, and T3, respectively. The numbers represent different types of forest: (1) continuous terra firme forest; (2) campinarana forest on paleochannel; (3) ecotonal forest; (4) seasonally flooded varzea forest. NMDS stress = 0.078.

than the adjacent flat plain areas covered by savanna vegetation. Although they have lower richness and diversity (Table 4), these two forest plots had floristic compositions that resemble the set of continuous forests in T1 and T2. Because they harbored some tree species of riverine and ecotonal (forest/savanna) habitats, their positions in the two axes of the NMDS diagram were slightly further away from the central group composed of the terra firme forests of T1 and T2 (Fig. 8). The most abundant trees in these two plots were *Goupia glabra* Aubl. (Celastraceae), *Iryanthera laevis* Markgr. (Myristicaceae), *Ruizterania retusa* (Spruce ex Warm.) Marc.-Berti (Vochysiaceae), *Pseudolmedia laevigata* Trécul (Moraceae), *Rudgea viburnoides* (Cham.) Benth (Rubiaceae), *Iryanthera paraensis* Huber (Myristicaceae), and *Mouriri nigra* (DC.) Morley (Melastomataceae), while the most abundant palms (Arecaceae) were *Euterpe precatoria* Mart., *Attalea speciosa* Mart., and *Oenocarpus minor* Mart.

HT04 consisted of a forest that differed floristically from all other forests in T1 and T2, as indicated by its isolated position in the cluster dendrogram and in the two-axis NMDS ordination (Figs. 7 and 8). The HT04 plot was from a site with paleomeander scars at the same topographic level as the adjacent savannas, and featured successional characteristics such as thinner and lower trees, a scarcity of epiphytes and lianas, and a large abundance of palms and secondary forest trees. The most abundant species recorded in this plot were the palms *Euterpe precatoria* Mart. and *Attalea speciosa* Mart. (Arecaceae), which represented 46% of the stems sampled in the plot, while the most common trees were the secondary growth species *Vismia sprucei* Sprague (Hypericaceae), *Guatteria olivacea* R.E.Fr. (Annonaceae), *Miconia acinodendron* (L.) Sweet (Melastomataceae), *Isertia* sp. (Rubiaceae), and *Schefflera* sp. (Araliaceae).

Among the forests that colonized the channel paleolandforms of unit T1, those from the areas still influenced by floods (HT02 and HT20; Fig. 9A–D) were characterized by species richness, diversity, and basal area much lower than in all other forests of the region (Table 4, Fig. 8). These plots were covered by campinarana forests (Fig. 9C, D) that transitioned to grasslands to the

Table 4. Floristic and structural characterization of the plots inventoried in the region of the middle Madeira River.

| Plot | Geom. unit | Forest type | Sedimentary substrate | Density (#/ha) | Basal area (m²/ha) | DAP (cm) (mean ± SD) | Tree height (m) (mean ± SD) | Richness | Shannon diversity |
|---|---|---|---|---|---|---|---|---|---|
| HT03 | T1 | Terra firme | Sandy channel | 690 | 33.8 | 20.5 ± 14.2 | 19.4 ± 9.1 | 60 | 3.8 |
| HT09 | T1 | Terra firme | Muddy (abandoned) channel/floodplain | 605 | 54.7 | 25.5 ± 22.4 | 23.8 ± 9.8 | 57 | 3.8 |
| HT12 | T1 | Terra firme | Muddy (abandoned) channel/floodplain | 610 | 22.5 | 19.4 ± 9.6 | 23.1 ± 8.3 | 39 | 3.1 |
| HT14 | T1 | Terra firme | Pebbly sandy channel | 428 | 48.5 | 28.8 ± 17.9 | 22.7 ± 9.2 | 59 | 3.8 |
| HT18 | T1 | Terra firme | Muddy (abandoned) channel/floodplain | 458 | 39.5 | 23.5 ± 18.1 | 22.6 ± 8.5 | 79 | 3.8 |
| HT02 | T1 | Campinarana | Muddy (abandoned) channel | 505 | 9.2 | 14.1 ± 5.6 | 14.5 ± 3.6 | 7 | 1.2 |
| HT20 | T1 | Campinarana | Sandy channel | 484 | 9.5 | 15.1 ± 4.6 | 18.3 ± 5.7 | 22 | 2.5 |
| HT04 | T2 | Terra firme | Muddy (abandoned) channel/floodplain | 650 | 18.5 | 17.6 ± 7.1 | 17.0 ± 5.3 | 25 | 2.3 |
| HT06 | T2 | Terra firme | Muddy (abandoned) channel/floodplain | 585 | 27.0 | 20.4 ± 13.1 | 16.6 ± 7.9 | 57 | 3.7 |
| HT11 | T2 | Terra firme | Sandy channel | 595 | 37.5 | 23.4 ± 16.1 | 20.9 ± 8.5 | 43 | 3.4 |
| HT16 | T2 | Terra firme | Muddy (abandoned) channel/floodplain | 408 | 23.0 | 22.7 ± 14.3 | 16.5 ± 5.8 | 83 | 4.1 |
| HT17 | T2 | Terra firme | Muddy (abandoned) channel/floodplain | 418 | 21.1 | 22.2 ± 12.3 | 19.6 ± 7.4 | 69 | 3.8 |
| HT26 | T2 | Terra firme | Muddy (abandoned) channel/floodplain | 372 | 34.7 | 29.3 ± 18.2 | 20.7 ± 7.2 | 41 | 3.1 |
| HT27 | T2 | Terra firme | Sandy channel | 250 | 22.9 | 27.9 ± 37.3 | 21.8 ± 7.8 | 56 | 3.7 |
| HT07 | T3 | Várzea forest | Muddy (abandoned) channel/floodplain | 460 | 37.2 | 24.6 ± 20.6 | 18.0 ± 9.3 | 64 | 4.0 |
| HT13 | T3 | Várzea forest | Sandy crevasse splay in muddy floodplain | 368 | 25.0 | 23.1 ± 18.3 | 16.6 ± 10.3 | 37 | 3.1 |

south along this feature (Fig. 9A, B) and contrasted with surrounding terra firme forests (Fig. 9E). The different floristic composition and structure of these plots were shown by a unique branch derived from the first cluster dendrogram node, supported by 100% bootstraps (Fig. 7), and by the wide separation from other forest stands on the x-axis of the NMDS diagram (Fig. 8B). We observed in the field that the substrates of HT02 and HT20 plots presented slightly concave-up morphologies that are flooded during the peak of wet seasons and intense rainfall events followed by storm water inflows. These paleochannels were directly connected to a drainage flowing to the southwest (Fig. 9B) and attributed to the inversion of former tributaries of the Madeira River (cf. Hayakawa and Rossetti 2015). The deposition of sediments within the channels continued even during the mid-/late Holocene (Bertani et al. 2015, see also Rossetti et al. 2017). The most abundant species of trees in these paleochannel

forests were *Vochysia divergens* Pohl (Vochysiaceae), *Ruizterania retusa* (Spruce ex Warm.) Marc.-Berti (Vochysiaceae), *Couma utilis* (Mart.) Müll.Arg. (Apocynaceae), *Hebepetalum humiriifolium* (G.Planch.) Benth. (Linaceae), *Goupia glabra* Aubl. (Celastraceae), and *Humiria balsamifera* Aubl. (Humiriaceae) In addition, the palm species *Euterpe precatoria* Mart. and *Mauritiella armata* (Mart.) Burret (Arecaceae) were present, which characterize many campinarana forests of the Amazonian lowlands.

Plot HT12 was from a site where a channel paleolandform was still visible in remote sensing images (Fig. 10A), although this site is no longer affected by seasonal flooding. As a result, the forest had floristic composition, diversity, and basal area intermediate between terra firme forests and campinarana forests on paleochannels of the plots HT02 and HT20, as evidenced by the position of these plots in the NMDS two-axis plot (Fig. 8; see also Fig. 10B–D). The most abundant tree species recorded in these plots were *Licania heteromorpha*
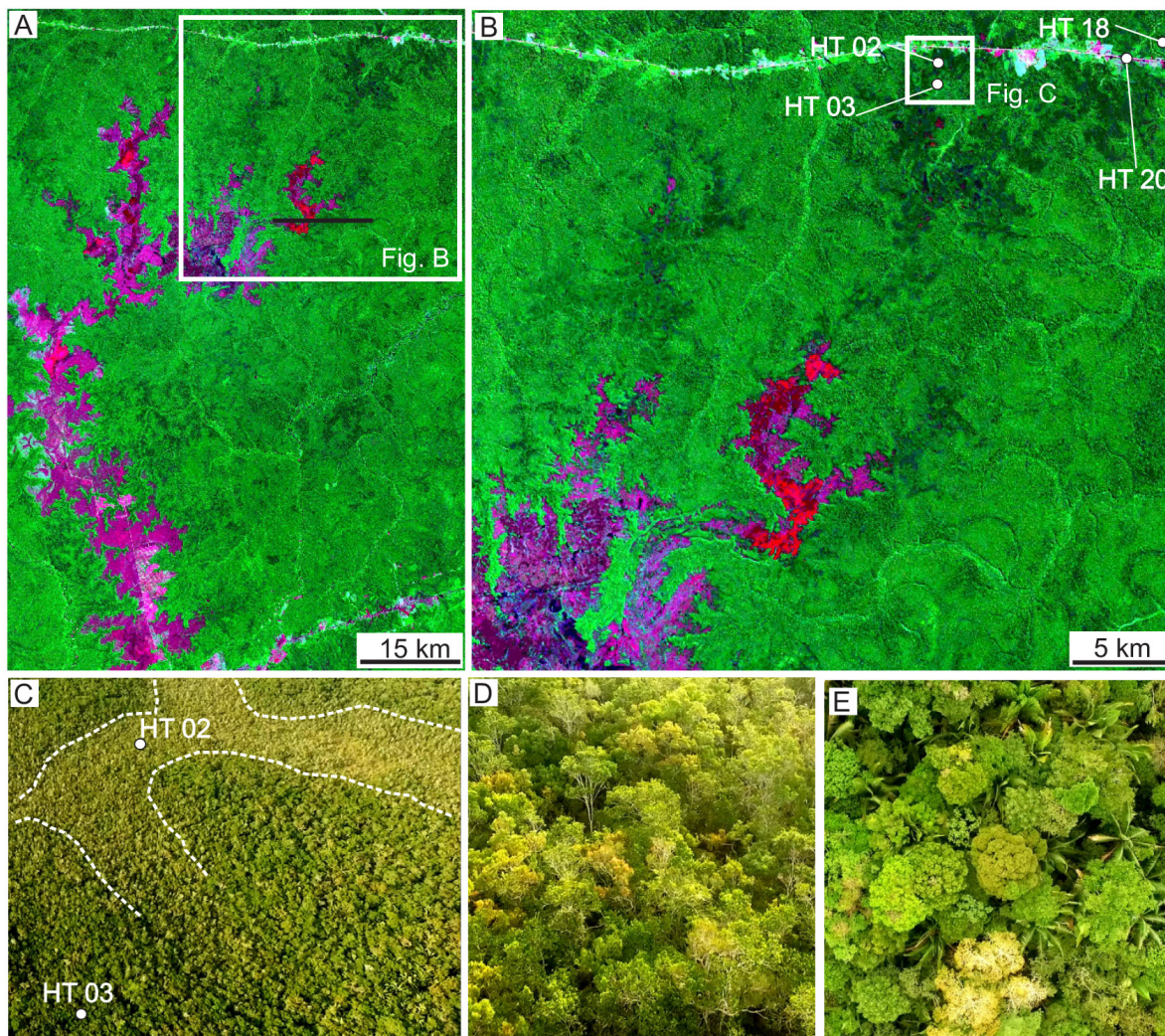
Fig. 9. Physiographic and floristic contexts of the plots HT02, HT03, HT18, and HT20. (A) Composite Landsat images with a broad view of the area under the influence of a paleolandform related to a drainage flowing to the south (purple and red = grassland/shrubland and exposed soil; light green = terra firme forest; dark green = white-sand vegetation on paleochannel). (B) Detail of A with the plots location, where HT02 and HT20 correspond to campinarana forests on paleochannels, and HT18 and HT20 are terra firme forests on surrounding interfluvial areas. (C) Details of the area containing the plots HT02 and HT03, with the first represented by campinarana forests on paleochannels (white dashed lines) and the latter represented by terra firme forests on interfluvial areas. (D) Detail of the campinara forest in the plot HT2. (E) Detail of the terra firme forest in the plot HT3. C to D are aerial drone photographs in orthogonal (C, E) and oblique views (D) (see Fig. 1 for location).

Benth. (Chrysobalanaceae), *Licania micrantha* Miq. (Chrysobalanaceae), *Qualea paraensis* Ducke (Vochysiaceae), *Vochysia divergens* Pohl (Vochysiaceae), *Ruizterania retusa* (Spruce ex Warm.) Marc.-Berti (Vochysiaceae), *Hirtella bicornis* Mart. & Zucc. (Chrysobalanaceae), and *Goupia glabra* Aubl. (Celastraceae), while the most abundant palms (Arecaceae) were *Oenocarpus bataua* Mart. and *Euterpe precatoria* Mart.

The two plots HT07 and HT13 (Fig. 11) of varzea forest of unit T3 presented a floristic composition considerably different from all forests in units T1 and T2, as indicated by their grouping in an independent branch with a bootstrap of 95% in
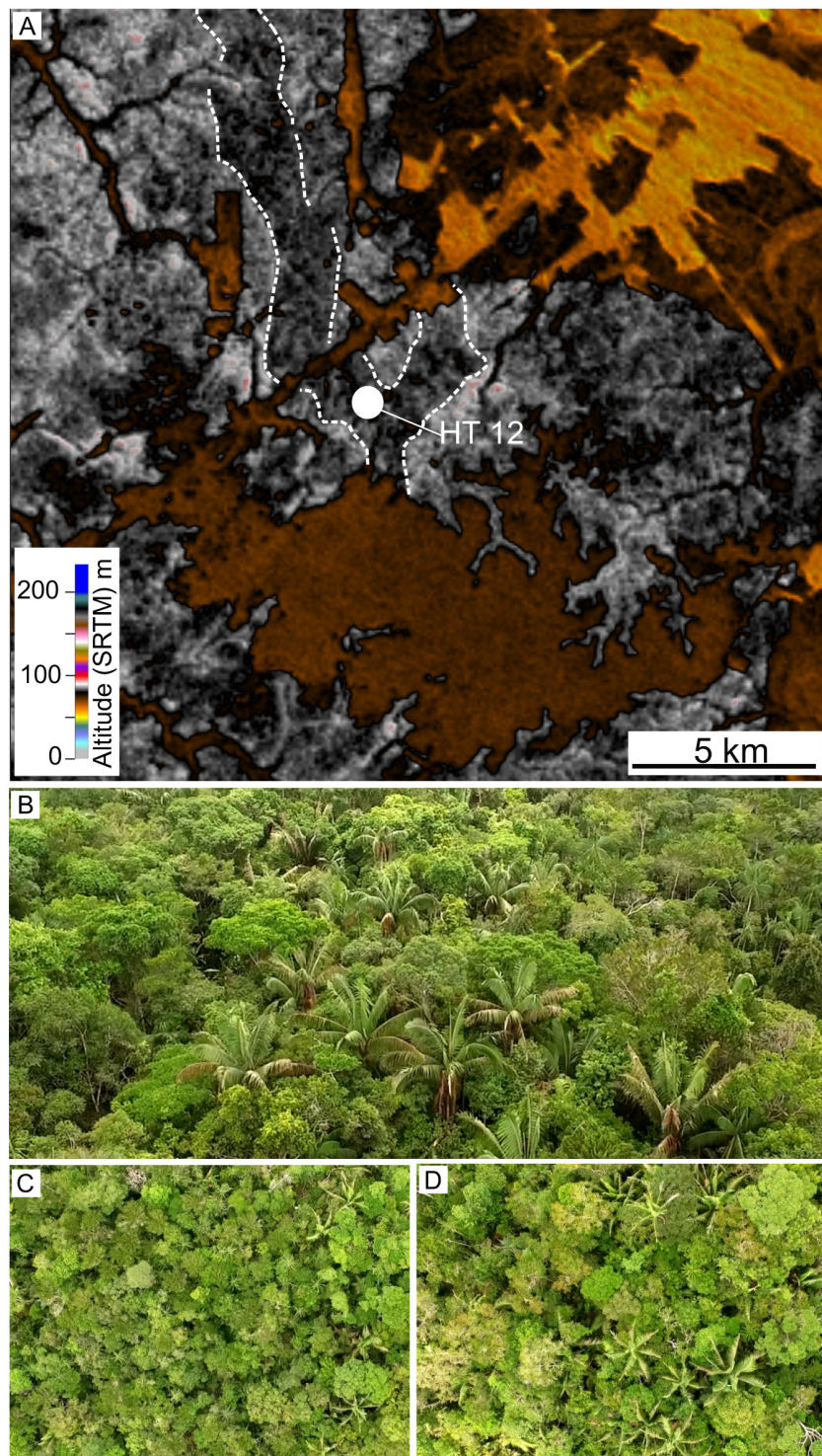
Fig. 10. Physiographic and floristic contexts of the plot HT12. (A) DEM-SRTM with the location of the plot

(Fig. 10. *Continued*)
HT12 in on elongated, branched paleolandform that presumably corresponds to a channel morphology (dark and light ocher areas = grasslands/shrublands; gray tons = forest; hatched lines = paleochannel). (B–D) Detail of the campinarana forest in the plot HT2 in oblique (B) and orthogonal views (C, D) based on drone photographs (see Fig. 1 for location).

the second node of the cluster dendrogram (Fig. 7). In addition, they were clearly differentiated by more negative values on the *y*-axis of the NMDS ordering diagram (Fig. 8). In contrast to the two plots of campinarana forest, the two plots of varzea forest presented diversity and species richness within the range of T1 and T2 terra firme forests (Table 4, Fig. 8B), with HT07 being the third more diverse among the studied forests (Fig. 2B). Likewise, the basal areas of the trees in this plot were the highest in the present study (Table 4, Fig. 8C). The species of trees with the greatest abundance in varzea forests were *Sloanea guianensis* (Aubl.) Benth. (Elaeocarpaceae), *Maquira coriacea* (H.Karst.) C.C.Berg. (Moraceae), *Apeiba echinata* Gaertn. (Tiliaceae), *Protium*



Fig. 11. Drone photograph illustrating the varzea forest of the T3 unit at the HT13 plot (see Fig. 1 for location).

*hebetatum* Daly (Burseraceae), *Pterocarpus rohrii* Vahl (Fabaceae), *Qualea paraensis* Ducke (Vochysiaceae), *Zygia juruana* (Harms) L.Rico (Fabaceae), and *Virola surinamensis* (Rol. ex Rottb.) Warb (Myristicaceae), while the *Astrocaryum murumuru* Mart. and *Attalea phalerata* Mart. ex Spreng. were the most common palm species (Arecaceae).

The forest types were not exclusive to a single lithology. For instance, neither the T1 and T2 continuous forests, nor the T2 ecotonal forests showed any preference for a sandy or muddy substrate (compare Figs. 2B and 3; see also Fig. 12). Despite the classification as campinarana forests, the paleochannel forests also presented several substrates that varied from sandy (HT20) to heterolithic bedded (HT02) or even muddy (HT12) sediments; only varzea forests were exclusive of muddy sediments. A comparison of the vegetation types of all sections studied, based on the integration of remote sensing information and eye drone views, confirmed the lithological independence of the various forests in the study area.

### $\delta^{13}C$ and C/N analyses

The sections selected for $\delta^{13}C$ and C/N analysis (Figs. 4–6) had values of $-28.66$ to $-14.38‰$ and 0.61 to 16.50, respectively, with upward variations independent of the lithological characteristics or depositional settings. Although depleted $\delta^{13}C$ and low to intermediate C/N generally predominated in all sections, there were also marked variations in some stratigraphic intervals worthy of description. Thus, deposits with OSL ages older than 43.0 ky were detected only in the lower half of section PV50A (Fig. 5), and were included in two successions of sandy channels with $\delta^{13}C$ depleted values of $-26.46$ to $-24.21‰$, with an upward enrichment. The corresponding C/N varied between 3.15 and 8.70, with a progressive decrease upwards. Sandy channel deposits with OSL ages equal to 36.6 ky occurred only at one site, that is, at the base of PV60A (Fig. 4), which had $\delta^{13}C$ and C/N between $-27.07$ and $-26.30‰$ and between 2.8 and 5.3, respectively, with both proxies decreasing in value upwards.

The deposits of the upper half of the section PV50A located in a site with ecotonal forests (Fig. 2B) recorded muddy floodplain and sandy crevasse splay environments. These deposits had a relative reduction of $\delta^{13}C$ up to $-27.31‰$ and lower C/N from 1.70 to 4.0 until 11,233 cal yr BP. The $\delta^{13}C$ was enriched to $-14.38‰$ in an
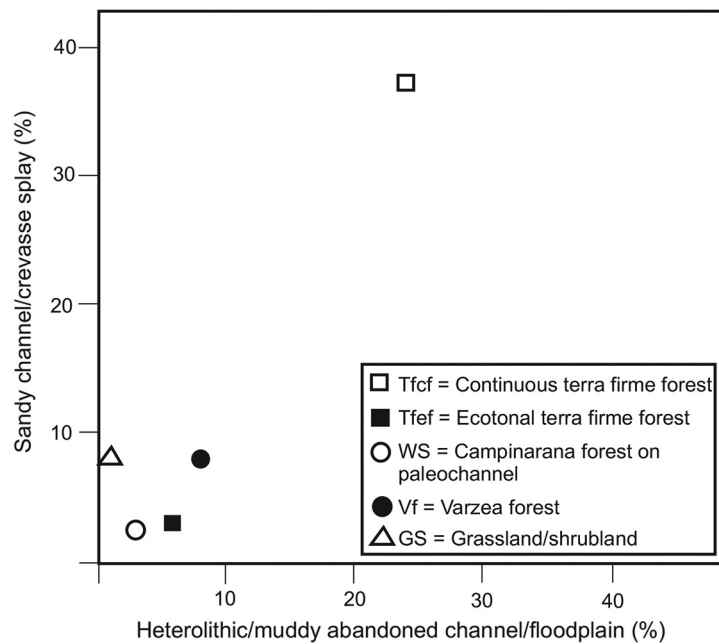


Fig. 12. Distribution of the different forests characterized in the study area according to substrate types.

estimated age of 1400 cal yr BP, with an upward return in more depleted values. This $\delta^{13}$C trend was accompanied by a gradual increase in C/N at the surface.

The low C/N with correspondingly depleted $\delta^{13}$C comparable to those recorded after 43 ky in section PV50A was also present in the lower and intermediate parts of the other sections of unit T2 and in all sections of unit T1 (Figs. 4 and 5); it is interesting to note that these intervals also consisted of muddy floodplain and sandy crevasse splay deposits. Another notable observation is that, similar to PV50A, all sections, except PV78A2, tended to increase $\delta^{13}$C and C/N values upwards, independently of the depositional environment of sandy/muddy channels or floodplains. Despite the general similarity in the curves, $\delta^{13}$C varied according to the location and proximity to modern savannas. Thus, $\delta^{13}$C values as enriched as −14.38‰ to −18.02‰ were recorded in the sections of ecotonal forests of T2 (i.e., PV50A, PV69A, and PV82A) and T1 (PV59A, PV60A). This proxy was as depleted as −21.28‰ and −25.36‰ in PV72A and PV73A, respectively, and both were located in T1. PV72A consisted of a campinarana forest on a channel paleolandform (Fig. 9C, D). In contrast, PV73A was located only 1.5 km from PV72A and <700 m from other areas of the paleochannel landform, but was covered by typical terra firme forest (Fig. 9E). The PV75A, which is a terra firme forest, also in unit T2 recorded the richest $\delta^{13}$C (−21.27‰), similar to PV72A. To top, the $\delta^{13}$C trend in all these sections resulted in relatively more depleted values, while C/N continued to increase, as in PV50A. Where ages were available, the time for enriched-depleted $\delta^{13}$C values in some of these sections was similar to this event in PV50A, that is, 11,573 cal yr BP in PV59A, and 11,189 cal yr BP in PV69A. This episode occurred earlier, that is, in ~20,000 cal yr BP in PV75A, later in 8734 cal yr BP in PV82A, and in 7578 cal yr BP in PV60A. Depletion in PV69A occurred almost at the same time as in PV50A, slightly older (i.e., 1624 cal yr BP) in PV60A and slightly later (i.e., after 964 cal yr BP) in PV59A. However, this event started as early as 3396 cal yr BP and 6130 cal yr BP in PV82A and PV75A, respectively.

The previously described enriched–depleted $\delta^{13}$C pattern was not recorded in the sections of T3, nor in PV78A2 of T1. In T3, dominated by varzea forests, $\delta^{13}$C vales ranged from −28.26 to −24.15‰, while this proxy varied even less (i.e., −28.66 to −26.29‰) in terra firme forests of PV78A2. C/N ranged widely from 0.61 to 13.00 in the T3 sections and from 4.63 to 8.73 in PV78A2. In all these sections, there was a sudden increase in C/N at the top, accompanied by a $\delta^{13}$C depletion tendency. These changes, initiated after estimated ages of 3402, 3174, and 2800 cal yr BP, became more effective after 1550, 1360, and 515 cal yr BP in the sections PV38, PV57, and PV58, respectively. The time for changes in $\delta^{13}$C and C/N in PV78A2 could not be determined because of the lack of dating in this section. However, other correlated deposits of this terrain were several thousand years old (Fig. 13). Thus, we speculate that the onset of the present-day forest in section PV78A2 may even have predated this event in the other sections.

## Discussion

### History of vegetation and time of the present-day forests

The non-random vertical distribution, the good correspondence of temporally equivalent deposits, and the lack of lithological control together motivated the use of $\delta^{13}$C and C/N of the sedimentary organic matter to interpret the past vegetation in the study area. Thus, a reconstruction of vegetation that existed before modern forests could be discussed, considering that C/N distinguishes between terrestrial (≥12.0) and aquatic (4.0–10.0) plants (e.g., Meyers 1997, Cloern et al. 2002, Wilson et al. 2005), while $\delta^{13}$C distinguishes $C_3$ (−32 to −20‰) from $C_4$ (−17 to −9.0‰) plants (Boutton 1996). The integration of these data with the characteristics of present-day forests in the study area allowed inferences about the vegetation dynamics in the context of environmental changes. We consider this fundamental understanding to discuss the factors that led to the change in vegetation over time and the establishment of the forests studied.

The prevalence of generally low C/N, particularly in the lower and middle parts of the studied sections, suggests a high contribution of algae and phytoplankton. This interpretation is compatible with the widespread development of aquatic environments consisting of river channels and
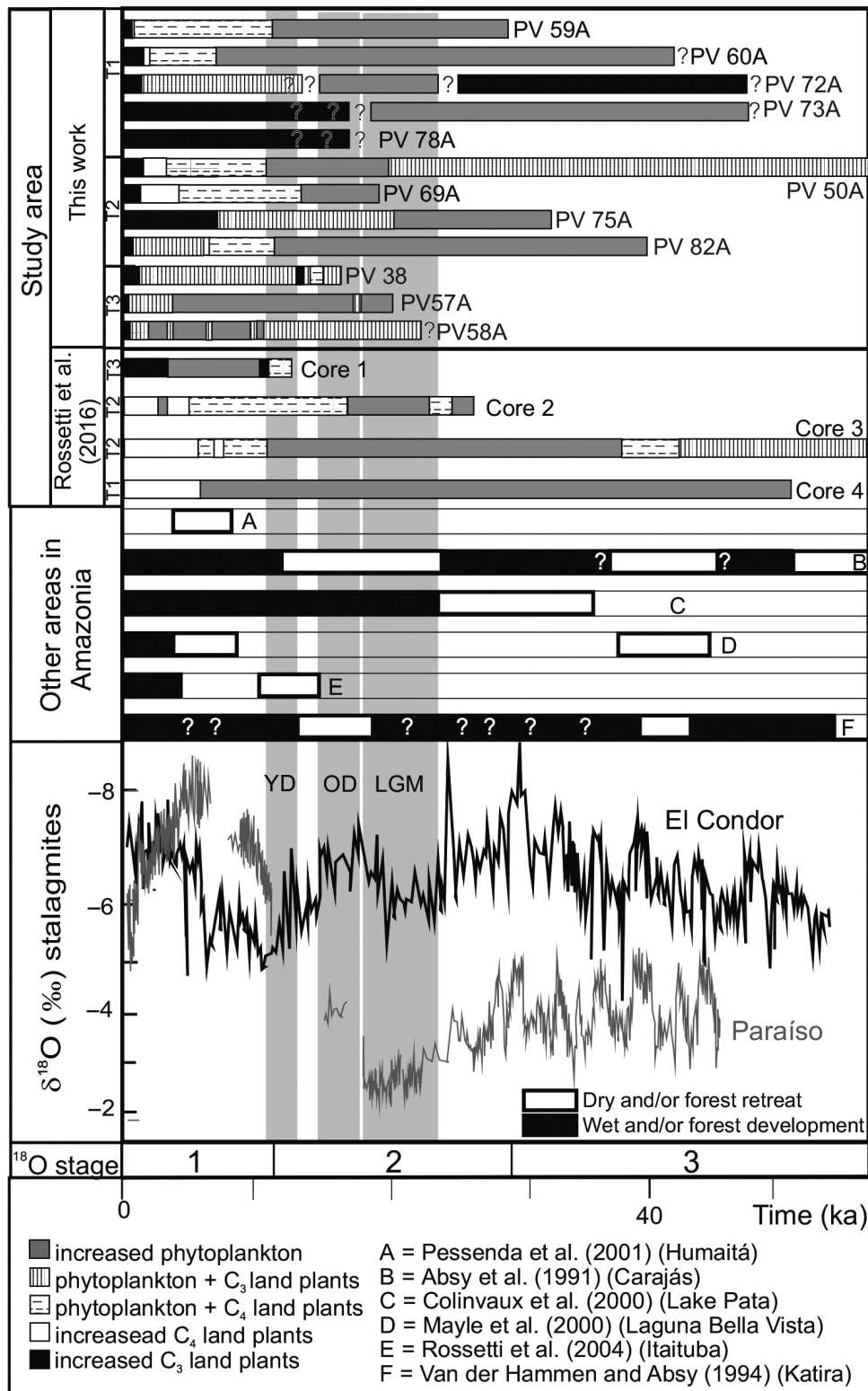
Fig. 13. Distribution of open and forest vegetation during the Last Glaciation compiled from several

(Fig. 13. *Continued*)
Amazonian areas, including data from the present work and previously published in Rossetti et al. (2014). The correspondence with major paleoclimatic episodes is included. $\delta^{18}O$ curve is from stalagmites of the Peruvian El Condor cave in western Amazonia (Cheng et al. 2013). The $\delta^{18}O$ stages 1 to 3 from are Emiliani (1955) and Shackleton (1969).

extensive floodplains. Channels that extend over a wide area, such as the Madeira River basin, have the potential to concentrate organic matter of terrestrial plants. The pulses and upward trend of C/N increased from 3.15 to 8.70 in deposits of sandy channels as old as 43 or 37 ky (e.g., PV50A and PV60A) probably indicate the contribution of terrestrial plants. The corresponding $\delta^{13}C$ values between $-26.46$ and $-24.21‰$ (PV50A) and between $-27.07$ and $-26.30‰$ (PV60A) suggest organic matter derived from plants with $C_3$ photosynthetic pathways. These values are relatively more enriched than those recorded in the leaves of the modern Amazonian forest trees, usually $<-29.7‰$ (cf. Ometto et al. 2006) or $<-28.9‰$ (cf. Francisquini et al. 2014), even assuming an isotopic fractionation of $3.0‰$ during the decomposition of organic matter in soils (Boutton 1996). In contrast, these values approach those of soils sampled from many tree savanna sites in this region, generally $>-25‰$ (Magnusson et al. 2002). These comparisons led to an inference that the rainforest and tree savanna could have contributed as sources to the organic matter deposited in the river channels before 43 ky. The depleted $\delta^{13}C$ and low C/N in deposits with ages between 43 ky and $\sim11$ cal ky BP of T2 and T3 indicate only phytoplankton with low or no inputs of terrestrial plants; an exception was PV75A, where this pattern ended at approximately 20 cal ky BP.

The subsequent trend in dominantly low C/N up to $\sim11$ cal ky BP in most sections and up to 7.5 cal ky BP in PV60A suggests depositional environments dominated by phytoplankton and low or no terrestrial plant inputs. If not coincidental, the prevalence of muddy floodplains and crevasse splays during this time interval suggests the amplification of low-energy environments away from land plant sources. However, the enriched-depleted $\delta^{13}C$ trend with the increase in C/N toward the top of all sections in units T1 and T2 (except PV78A2) shows some variations that require clarification. The increase in C/N reveals a greater contribution of terrestrial plants over

time. The intervals with $\delta^{13}C$ up to $-14.38‰$ or at least $-18.02‰$ in some T2 (PV50A, PV69A, and PV82A) and T1 (PV59A, PV60A) sections are related to the increase in $C_4$ terrestrial plant inputs. This interpretation is consistent with the fact that these sections are from campinarana or ecotonal forests found on paleochannels. Thus, broader areas of savanna probably existed before the present-day forests, a process initiated at $\sim11,000$ cal yr BP in most sections, earlier in $\sim20,000$ cal yr BP in PV75A, and later in 7578 cal yr BP in PV60A. The $\delta^{13}C$ enriched-depleted trends in PV72A and PV73A also attest changes in past vegetation, but higher values of only $-21.28‰$ and $-25.36‰$, respectively, prevented the confirmation of a direct relationship with $C_4$ terrestrial plants in these sites. These values suggest a degree of disturbance in past forests more open than the modern canopy. The past forests, particularly in PV72A, had values compatible with Amazonian tree savanna soils (Magnusson et al. 2002, Francisquini et al. 2014). The beginning of this vegetation type could not be dated in PV73A, but occurred at the end of the Holocene after deposition of the channel in PV72A. Values of $\delta^{13}C$ up to $-21.27‰$ on the PV75A substrate suggest a relatively more open past vegetation structure than the current terra firme forest of this site.

The depleted $\delta^{13}C$ and the low-to-intermediate C/N in T3 indicate that $C_4$ terrestrial plants did not develop in areas closer to the Madeira River, which remained dominated by phytoplankton or a mixture of phytoplankton and $C_3$ terrestrial plants (probably from varzea forests) over this time interval. The values of $\delta^{13}C$ as low as $-26.13$ to $-28.66‰$ in PV78A are also compatible with the absence or low contribution of this type of plant in the deposits of unit T1 east of the Madeira River.

We infer that the increase in depletion of $\delta^{13}C$ in all sections studied, while C/N continued to increase, marks the colonization of terrestrial grasses followed by present-day forests. The

beginning of forestation on several occasions between 6130 and 964 cal yr BP attests to long-term disturbances. However, a simple pattern of variation in plant communities was not detected, even when comparing temporally equivalent deposits located over short distances, which makes it difficult to determine the driver (s) of environmental disturbances.

*Linkage to past climate*

The upsurge of grasslands and their transition to present-day terra firme and ecotonal forests should be analyzed together when relating the contrasting vegetation in the study area to long-term disturbances. The increase in the contribution of $C_4$ terrestrial plants before present-day forests is remarkable, particularly considering the forest onsets at various ages between 11,189 and 11,573 cal yr BP (Fig. 13), that is, near the Younger Dryas (YD) between 12,900 and 11,700 cal yr BP (cf. Carlson 2013). The imprint of this event in South America remains to be investigated in greater depth. However, there is a suggestion that the extensive savanna of the Gran Sabana in the Orinoco region of northern Amazonia occurred during this climatic event, followed by the amplification of the Holocene savanna due to anthropogenic fires (Rull et al. 2017). The record of $C_4$ terrestrial plants has been used to suggest dry periods in other Amazonian areas, not only in the YD, but also in the Last Glacial Maximum (LGM) and Oldest Dryas (OD; e.g., Absy et al. 1991, van der Hammen and Absy 1994, Mayle et al. 2000, Colinvaux et al. 2000).

The grassland vegetation of the study area was interpreted as relics of dry climatic episodes from early to mid-Holocene (Freitas et al. 2001, Pessenda et al. 2001). A recent publication, however, recorded its asynchronous development in the mid-late and late Holocene (Rossetti et al. 2016). Rather than due to climatic changes, these authors also related the establishment of this vegetation type to sedimentary dynamics, because: these grasslands are confined to fluvial landforms; global humidity increased >40% after the YD (Maslin and Burns 2000); pollen data indicated forestation in many other Amazonian areas when savannas were formed (e.g., Absy et al. 1991, Colinvaux et al. 2000, Mayle et al. 2000, Toledo and Bush 2008; Fig. 13). In addition, several grasslands of considerable dimension are mixed with forests in the modern landscape of this equatorial region (e.g., Adeney et al. 2016); thus, relating past grasslands to dry climates is a simplified interpretation.

The new discovery of grasslands in the YD, as well as before the mid-Holocene (PV60A and PV82A) and in the LGM (section PV75A; Fig. 13), supports the idea that climate was not the main driver for the establishment of grasslands in the Madeira region. Pollen data of the studied area indicated a cold but humid climate before the LGM between >42,600 and <35,200 cal yr BP, as well as grasslands and forests representative of modern tree species, which suggest a climate comparable to today's, at least during the Holocene (Cohen et al. 2014). However, since the late Quaternary climatic data from the lowlands of Amazonia are still few and contradictory (Fig. 13), independent paleoclimatic data are needed to confirm these climatic patterns.

Paleoclimatic reconstructions based on $\delta^{18}O$ of speleothems pointed to opposite climatic patterns when comparing data from western and eastern Amazonian caves. Thus, the data of the Paraíso cave in the eastern Amazonia (4°4′ S, 55°27′ W) indicated reduced humidity between 45 and 18 ky, with a trend of 60% compared to current levels during the LGM (Wang et al. 2017, see the gray curve in Fig. 13). These authors recorded enriched $\delta^{18}O$ of $-3.0‰$ between 19 and 21 ky, when the rainforest probably persisted with a reduced tree cover. Then, the $\delta^{18}O$ was depleted to the modern level of $-6.0‰$, but with a peak of $-8.7‰$ between 6 and 5 ky, when precipitation was probably 142% higher than current levels. Data from the Peruvian caves of Diamante (5°44′ S/77°30′ W) and El Condor (5°56′ S/77°18′ W) in western Amazonia, however, indicated a wet LGM followed by a moderately dry last interglacial period for the early/mid-Holocene, when $\delta^{18}O$ reached values as enriched as $-4‰$ (Cheng et al. 2013, see the black curve in Fig. 13). The increase in humidity in the region began 5 ky ago and culminated in values of $\delta^{18}O$ from $-6$ to $-7‰$, which is only slightly more depleted than the LGM levels. The shifts in the position of the Intertropical Convergence Zone (ITCZ) under the influence of the Atlantic Meridional Ocean Circulation were claimed as the cause for the east-to-west gradient in humidity over the lowlands of Amazonia since the beginning of the LG (Wang et al. 2017).

Whether the changes in the ITCZ also affected the central and southern Amazonian areas in past geological times is unknown (Wang et al. 2017). An increased eastward depletion in $\delta^{18}O$ of $-1‰$ per 1000 km is estimated as a result of the ITCZ displacement, but this displacement decreases over time when data from the Amazonian caves are contrasted (Wang et al. 2017). Based on these premises, it is most likely that the study area, located ~1500 km west of the cave of Paraíso and ~1300 km of the Peruvian caves, presented humidity levels that contrasted less with current levels before and during the LG and subsequent interglacial stages. This interpretation is consistent with the record of forests in the study area over the last ~40,000 cal yr BP, as suggested by the pollen data. The paleoclimatic scenario also agrees with the proposals of a relatively undisturbed Amazonian forest over the last 50,000 yr (e.g., Colinvaux et al. 1996, 2000, Colivaux et al. 2001, Bush et al. 2004, Irion et al. 2006, Mayle and Power 2008, Toledo and Bush 2008). The abundance of aquatic environments with high phytoplankton content in the studied sections is compatible with moisture throughout the deposition time.

*Potential driver of vegetation change in space and time*

We postulate that factors other than just climate influenced the beginning of the grasslands and, later, the types of forest studied, with a suitable hypothesis involving the soil. However, an earlier publication that focused more on contrasting forest and savanna vegetation revealed soils in the study area with similar chemical and identical mineralogical attributes (Martins et al. 2006). Thus, factors other than soil should also be considered.

The episodes of grassland expansion in the study area should be analyzed considering that grasslands: that existed prior to present-day forests were recorded in all sections of T2 but only in two sections of T1 (i.e., PV59A, PV60A) and none in T3; grasslands occur on the modern landscape of T1 and T2, but not of T3; most of this formation is confined to fluvial paleolandforms (see also Bertani et al. 2015); all sections of T2 and two sections of T1 with past grassland records are adjacent to areas currently colonized by this type of vegetation; and the grassland records in the two sections of T1 were not synchronous, occurring at ~11 cal ky BP and 7.5 cal ky BP in PV59A and PV60A, respectively. All data together suggest a clear connection between past and present-day grasslands. Thus, the most probable scenario is that units T1 and T2 had areas of savanna that diminished in size from the mid-Holocene by their replacement by forests. If this interpretation is correct, the ecotonal and campinarana forests on paleochannels would record younger and less mature communities of lower diversity than the terra firme forests, because they are in an intermediate successional stage between savannas and terra firme forests.

More sites are still needed to improve our database, but a relationship between forest maturity and time could be invoked by T1 terra firme forests with a higher basal area and taller trees than similar forests in relatively younger deposits of T2, as well as lower species diversity of the ecotonal and campinarana forests on paleochannels, both with substrates younger than those of terra firme forests. This interpretation is consistent with the earlier onset (6130 cal yr BP) of terra firme forests compared to ecotonal and campinarana forests on paleochannels (between 3396 and 964 cal yr BP).

However, forests can only take 100–400 yr to reach maturity (Guariguata and Ostertag 2001), with a proposed threshold of 450 yr (Liu et al. 2014). Taking into account these ages, all forests studied should exhibit highly diversified communities, considering their time of formation between 6130 and 964 cal yr BP. On the other hand, a recent research (i.e., Martin et al. 2016) stated that a threshold age for forest maturity may not exist because many factors beyond time influence forest development, such as temperature and precipitation (Anderson et al. 2006, Anderson-Teixeira et al. 2013), extreme climatic events (Wright 2005), seasonality (Zemp et al. 2017), or anthropogenic interferences (Norden et al. 2015, Levis et al. 2017).

We postulate that time may have had only an indirect influence on the maturity of the forest in the study area. The most probable explanation is that the downcutting and deposition of terraces along the Madeira River due to tectonic reactivation (cf. Rossetti et al. 2014) might have played a fundamental hole in the distribution of savanna and forests over time. This

interpretation is consistent with the fact that diversified terra firme forest communities with higher trees and greater basal areas were restricted to stable surfaces of T1, where sediment deposition was deactivated long ago. As a consequence of sedimentary dynamics, these sites were also not disturbed in topographically higher positions, remaining above the water table, even during humid peak seasons. The undisturbed environment would have kept the terra firme forests stable over time, allowing the regeneration of the trees to follow complete successional stages into the terra firme forests. However, renewed sedimentation in this plateau by subsequent river dynamics locally disturbed existing forests, as recorded, for instance, by the campinarana forests on paleochannels (parcels HT2, HT20, and HT12). These plots are, respectively, of sections PV72A, PV105A, and PV59A, which end up in sedimentary successions formed by renewed channeling renovation later than the depositional surface T1. The first two sections record an earlier tributary network of the Madeira River (Fig. 1A, B). The segments of this paleodrainage south of the study area consist of sandy channels that transited to muddy fluvial rias, with sediment deposition continuing at least until the mid-/late Holocene (Bertani et al. 2015, Rossetti et al. 2017). This environmental disturbance in a geologically recent time seems to be still imprinted in the modern landscape. This is suggested by our personal observation that PV72A remains inundated longer during wetter seasons than adjacent lands. This is also suggested by the gradation of present campinarana forests into grasslands to the south along the paleodrainage. It is interesting that PV73A, although located only 1.5 km from PV72A, has a continuous terra firme forest, which can be explained by its external position to the paleochannel landform of PV72A (Fig. 1C). In addition, the values of $\delta^{13}C$ $-25.36‰$ along PV73A indicate terra firme forests with a more open canopy than the one present, which were related to environmental disturbances caused by intermittent overbank sedimentation in the floodplains adjacent to the channels. The occurrence of PV59A in a channel paleolandform no longer affected by seasonal flooding (differently from PV72A and PV105A) may justify a vegetation with composition,

diversity, and basal area intermediate between the terra firme and campinarana forests of the plots HT02 and HT12. In comparison, the depleted peak of $\delta^{13}C$ to $-21.27‰$ in the PV78A (HT09) terra firme forest plot could also be an indication of tree savanna vegetation before the establishment of the present-day forest.

The various vegetation patterns of T2 provided additional elements to support the proposed influence of time and environmental changes on the spatial distribution of the studied forests. The location of continuous forests from the plots HT06, HT16, HT17, and HT27 on substrates older than 3533 cal yr BP could suggest a relationship with time. Such an interpretation would be consistent with the fact that PV75A, also a site of continuous terra firme, recorded a turnover from savanna to forest at 6130 cal yr BP. However, the ages of this event between 1624 and 964 cal yr BP in the ecotonal forests (PV50A, PV69A, and PV82A) should have led to forest maturity, considering the 450-yr forest maturity threshold of Liu et al. (2014). In addition, the plot HT4 on substrates as old as 14,458 cal yr BP reinforces the claim that forest development occurred in a relatively recent time because, despite the old substratum, this parcel is in an ecotonal forest with even thinner and smaller trees and poorer epiphytes and lianas than similar forests in T2. We postulate that, instead of time, the lower topographic location in relation to T1 due to progressive terrace downcutting explains the coexistence of terra firme and ecotonal forests in T2. Although protected against seasonal floods, this terrain is closer to the Madeira River than T1, thus it could have been more affected by exceptional floods. For instance, the historical floods of this river in 2014 raised the water level more than 20 m, inundating a large area located more than 20 km from the main river course (e.g., http://www.ceped.ufsc.br/2014-cheia-do-rio-madeira-afeta-rondonia-acre-e-amazonas/). Similar floods were recorded only in 1997 (cf. http://maisro.com.br/sipam-garante-que-nova-enchente-recorde-do-madeira-so-daqui-a-180-anos/). Based on this information, we infer that comparable flood events may have occurred in past geological times, probably keeping many areas on the surface of T2 flooded. We speculate that this is why T2 had larger areas of grasslands in the former and modern landscape, where they remain

flooded during the wet seasons. As a result, all sites close to this open vegetation (i.e., all sections in T2 except PV75A) are covered by ecotonal forests because they are influenced by hydrological disturbances caused by eventual flood events.

Unit T3 is located closer to the Madeira River in a location more susceptible to frequent inundations than the other geomorphological units. Consequently, T3 is dominated by flood-tolerant species, such as those of the plots HT07 and HT13. The deposition of $C_3$ terrestrial plants between 3402 and 2800 cal yr BP in this terrain, revealed by the increase in C/N values, probably occurred when the Madeira River cut down the lower T3 unit. As expected, C3 terrestrial plants were mixed with abundant aquatic plants due to the gradual abandonment of subaqueous depositional environments, such as channels and floodplains. The increased sign of $C_3$ terrestrial plants with more depleted $\delta^{13}C$ values at ~1550 cal yr BP shows the earlier development of varzea forests in T3.

A recent publication suggested that the evolution of savannas and forests in the central and southern Lhanos de Moxos in Bolivian Amazonia was due to changes in fluvial environments by tectonic reactivation during the Holocene (Lombardo 2014). Likewise, the history of Late Pleistocene–Holocene terrace downcutting and deposition along the Madeira valley has been related to reactivations along the Madre de Dios-Itacoatiara Transcurrent Fault Zone (Souza–Filho et al. 1999, Rossetti et al. 2014). This geological process, which seems to have continued even in recent geological times as evidenced by a 1341 cal yr BP seismite (Rossetti et al. 2017), would have favored the topographic gradients that were fundamental to control the hydrology and distribution of vegetation communities in the study area.

## Conclusions and Ways Forward

Our study concludes that neither climate nor mineralogical or edaphic changes can explain the past savannas or the present-day distribution of various types of forest in the study area. In fact, the onsets of savanna, a phytophysiognomy still present within the rainforest matrix, occurred at different times ranging from the LGM to the mid-Holocene, regardless of climate. In the same way, the various types of forest were formed at different ages between 6130 and 964 cal yr BP. The evolution of fluvial terraces, perhaps, controlled by tectonic reactivations, seems to have been fundamental for the creation of in situ topographic gradients and consequent hydrologic variations at various scales. We propose that these environmental changes, rather than the time of forest maturity, were fundamental to the establishment of various types of forest and their maintenance over the landscape under study. Savannas decreased in size over time, with replacement by forests.

The results of the present study point to the need to reinforce initiatives aimed at the conservation of tropical areas in terrains with complex sedimentary histories. In the study area, hydrological gradients shaped different types of habitats, with transitions from forests to savannas, which increased the biodiversity considering the landscape as a whole. Our data suggest that long-term secondary succession processes dating back to Late Pleistocene led to the progressive replacement of savannas by forests, with the consequent increase in biomass in older terrains. We concluded that environmental heterogeneities contributes in a way that has not yet been measured by studies aiming the conservation of Amazonian biodiversity and atmospheric carbon sink.

It is worth noting that this work considered only pristine forests and disregarded second-growth anthropogenic forests that were also present in the study area. Ancient anthropogenic forests from the management by the Amerindians, such as the dense aggregations of Brazil nut trees (*castanhais*), were also avoided in this study. However, we recommend further investigation that can consider also human influences in the structure and floristic composition of the terraces studied along the Madeira River.

## Literature Cited

Absy, M. L., et al. 1991. Mise en évidence de quatre phases d' ouverture de la forêt dense dans le sud-est de L'Amazonie au tours des 60.000 dernières années. Première comparaison avec d'autres régions tropicales. Comptes Rendus de l'Académie des Sciences Paris (Series II) 312:673–678.

Adeney, J. M., N. L. Christensen, A. Vicentini, and M. Cohn-Haft. 2016. White-sand ecosystems in Amazonia. Biotropica 48:7–23.

Anderson, K. J., A. P. Allen, J. F. Gillooly, and J. H. Brown. 2006. Temperature-dependence of biomass accumulation rates during secondary succession. Ecology Letters 9:673–682.

Anderson-Teixeira, K. J., A. D. Miller, J. E. Mohan, T. W. Hudiburg, B. D. Duval, and E. H. Lucia. 2013. Altered dynamics of forest recovery under a changing climate. Global Change Biology 19:2001–2021.

Baker, P. J., S. Bunyavejchewin, C. D. Oliver, and P. S. Ashton. 2005. Disturbance history and historical stand dynamics of a seasonal tropical forest in western Thailand. Ecological Monographs 75:317–343.

Baker, P. A., S. C. Fritz, C. W. Dick, A. J. Eckert, B. K. Horton, S. Manzoni, C. C. Ribas, C. N. Garzione, and D. S. Battisti. 2014. The emerging field of geogenomics: constraining geological problems with genetic data. Earth-Science Reviews 135:38–47.

Bertani, T. C., D. F. Rossetti, E. H. Hayakawa, and M. C. L. Cohen. 2015. Understanding Amazonian fluvial rias based on a Late Pleistocene-Holocene analog. Earth Surface Processes and Landforms 40:285–292.

Boutton, T. W. 1996. Stable carbon isotope ratios of soils organic matter and their use as indicators of vegetation and climate change. Pages 47–82 in T. W. Boutton and S. I. Yamasaki, editors. Mass spectrometry of soils. Marcel Dekker, New York, New York, USA.

Bray, J. R., and J. T. Curtis. 1957. An ordination of the upland forest communities of Southern Wisconsin. Ecological Monographs 27:325–349.

Burslem, D. F. R. P., T. C. Whitmore, and G. C. Brown. 2000. Short-term effects of cyclone impact and long-term recovery of tropical rainforest on Kolombangara, Solomon Islands. Journal of Ecology 88:1063–1078.

Bush, M. B. 1994. Amazonian speciation: a necessarily complex model. Journal of Biogeography 21:5–17.

Bush, M. B., P. E. Oliveira, P. A. Colinvaux, M. C. Miller, and J. E. Moreno. 2004. Amazonian palaeoecological histories: One hill, three watersheds. Palaeogeography, Palaeoclimatology, Palaeoecology 214:359–393.

Carlson, A. E. 2013. The Younger Dryas climate event. Encyclopedia of Quaternary Science 3:126–134.

Cheng, H., A. Sinha, F. W. Cruz, X. Wang, R. L. Edwards, F. M. d'Horta, C. C. Ribas, M. Vuille, L. D. Stott, and A. S. Auler. 2013. Climate change patterns in Amazonia and biodiversity. Nature Communications 4:1411.

Chikaraishi, Y., and H. Naraoka. 2006. Carbon and hydrogen isotope variant of plant biomarkers in a plant-soil system. Chemical Geology 231:190–202.

Clark, D. B., D. A. Clark, and S. F. Oberbauer. 2010. Annual wood production in a tropical rainforest in NE Costa Rica linked to climatic variation but not to increasing $CO_2$. Global Change Biology 16:747–759.

Clarke, K. R. 1993. Non-parametric multivariate analyses of changes in community structure. Australian Journal of Ecology 18:117–143.

Clarke, K. R., and R. H. Green. 1988. Statistical design and analysis for a 'biological effects' study. Marine Ecology Progress Series 46:213–226.

Cloern, J. E., E. A. Canuel, and D. Harris. 2002. Stable carbon and nitrogen isotope composition of aquatic and terrestrial plants of the San Francisco Bay Estuarine System. Limnology and Oceanography 47:713–729.

Cohen, M. C. L., D. F. Rossetti, L. C. R. Pessenda, Y. S. Friaes, and P. E. Oliveira. 2014. Late Pleistocene glacial forest of Humaitá-western Amazônia. Palaeogeography, Palaeoclimatology, Palaeoecology 415:37–47.

Colinvaux, P. A., P. E. Oliveira, and M. B. Bush. 2000. Amazonian and neotropical plant communities on glacial time-scales: the failure of the aridity and refuge hypotheses. Quaternary Science Reviews 19:141–169.

Colinvaux, P. A., P. E. Oliveira, J. E. Moreno, M. C. Miller, and M. B. Bush. 1996. A long pollen record from lowland Amazonia: forest and cooling in glacial times. Science 274:85–88.

Colivaux, P. A., G. Irion, M. E. Räsänen, M. B. Bush, and J. A. S. N. Mello. 2001. A paradigm to be discarded: Geological and paleoecological data falsify the Haffer and Prance refuge hypothesis of Amazonian speciation. Amazoniana 16:609–646.

Daïnou, K., J. P. Bizoux, J. L. Doucet, G. Mahy, O. J. Hardy, and M. Heuertz. 2010. Forest refugia revisited: NSSRs and cpDNA sequences support historical isolation in a wide-spread African tree with high colonization capacity, Milicia excelsa (Moraceae). Molecular Ecology 19:4462–4477.

Deines, P. 1980. The isotopic composition of reduced organic carbon. Pages 329–406 in P. Fritz and J. C. Fontes, editors. Handbook of environmental isotope geochemistry. Elsevier, New York, New York, USA.

Duller, G. A. T. 2004. Luminescence dating of Quaternary sediments: recent advances. Journal of Quaternary Science 19:183–192.

Emiliani, C. 1955. Pleistocene temperatures. Journal of Geology 63:538–578.

Espírito-Santo, F. D. B., M. Keller, B. Braswell, B. W. Nelson, S. Frolking, and G. Vicente. 2010. Storm intensity and old-growth forest disturbances in the Amazon region. Geophysical Research Letters 37: L11403.

Fine, P. V. A., R. Garcia-Villacorta, N. C. A. Pitman, I. Mesones, and S. W. Kembel. 2010. A floristic study of the white-sand forests of Peru. Annals of the Missouri Botanical Garden 97:283–305.

Fortunel, C., C. Paine, P. V. Fine, N. J. Kraft, and C. Baraloto. 2014. Environmental factors predict community functional composition in Amazonian forests. Journal of Ecology 102:145–155.

Francisquini, M. I., C. M. Lima, L. C. R. Pessenda, D. F. Rossetti, M. C. Franca, and M. C. L. Cohen. 2014. Relation between carbon isotopes of plants and soils on Marajó Island, a large tropical island: implications for interpretation of modern and past vegetation dynamics in the Amazon region. Palaeogeography, Palaeoclimatology, Palaeoecology 415:91–104.

Freitas, H. A., L. C. R. Pessenda, R. Aravena, S. E. M. Gouveia, A. S. Ribeiro, and R. Boulet. 2001. Late Quaternary vegetation dynamics in the southern Amazon Basin inferred from carbon isotopes in soil organic matter. Quaternary Research 55:39–46.

Galbraith, R. F., and P. F. Green. 1990. Estimating the component ages in a finite mixture. Nuclear Tracks and Radiation Measurements 17:197–206.

Galbraith, R. F., and R. G. Roberts. 2012. Statistical aspects of equivalent dose and error calculation and display in OSL dating: an overview and some recommendations. Quaternary Geochronology 11:1–27.

Garcin, Y., et al. 2014. Reconstructing $C_3$ and $C_4$ vegetation cover using n-alkane carbon isotope ratios in recent lake sediments from Cameroon, Western Central Africa. Geochimica et Cosmochimica Acta 142:482–500.

Gottsberger, G., and W. Morawetz. 1986. Floristic, structural and phytogeographical analysis of the savannas of Humaitá (Amazonas). Flora 178:41–71.

Guariguata, M. R., and R. Ostertag. 2001. Neotropical secondary forest succession: changes in structural and functional characteristics. Forest Ecology and Management 148:185–206.

Guitét, S., V. Freycon, O. Brunax, R. Pélissier, D. Sabatier, and P. Couteron. 2016. Geomorphic control of rain-forest floristic composition in French Guiana: More than a soil filtering effect? Journal of Tropical Ecology 32:22–40.

Haugaasen, T., and C. A. Peres. 2006. Floristic, edaphic and structural characteristics of flooded and unflooded forests in the lower Rio Puru's region of central Amazonia, Brazil. Acta Amazonica 36:25–35.

Hayakawa, E. H., and D. F. Rossetti. 2015. Late Quaternary dynamics in the Madeira River basin, southern Amazonia (Brazil), as revealed by paleomorphological analysis. Anais da Academia Brasileira de Ciências 87:29–49.

Hayakawa, E. H., D. F. Rossetti, and M. M. Valeriano. 2010. Applying DEM–SRTM for reconstructing a late Quaternary paleodrainage in Amazonia. Earth and Planetary Science Letters 297:262–270.

Higgins, M. A., K. Ruokolainen, H. Tuomisto, N. Llerena, G. Cardenas, O. L. Phillips, R. Vásquez, and M. Räsänen. 2011. Geological control of floristic composition in Amazonian forests. Journal of Biogeography 38:2136–2149.

IBGE. 2012. Manual técnico da vegetação brasileira: sistema fitogeográfico, inventário das formações florestais e campestres, técnicas e manejo de coleções botânicas, procedimentos para mapeamentos. IBGE. Second edition. Instituto Brasileiro de Geografia e Estatística, Rio de Janeiro, Rio de Janeiro, Brazil.

Irion, G., M. B. Bush, J. A. N. Mello, D. Stüben, T. Neumann, R. G. Müller, J. O. Moraes, and J. W. Junk. 2006. A multiproxy palaeoecological record of Holocene lake sediments from the Rio Tapajós, eastern Amazonia. Palaeogeography, Palaeoclimatology, Palaeoecology 240:523–536.

Krustal, J. B., and M. Wish. 1978. Multidimensional scaling. Sage University Paper Series on Quantitative Applications in the Social Sciences, Sage Publications, University of Iowa, Iowa city, Iowa, USA.

Lebamba, J., A. Vincens, and J. Maley. 2012. Pollen, vegetation change and climate at Lake Barombi Mbo (Cameroon) during the last ca. 33 000 cal yr BP: a numerical approach. Climate of the Past 8:59–78.

Latrubesse, E. M. 2002. Evidence of Quaternary palaeohydrological changes in middle Amazônia: The Aripuanã-Roosevelt and Jiparaná "fans". Zeitschrift für Geomorphologie 129:61–72.

Levis, C., et al. 2017. Persistent effects of pre-Columbian plant domestication on Amazonian forest composition. Science 355:925–931.

Liu, Y., G. Yu, Q. Wand, and Y. Zhang. 2014. How temperature, precipitation and stand age control the biomass carbon density of global mature forests. Global Ecology and Biogeography 23:323–333.

Lombardo, U. 2014. Neotectonics, flooding patterns and landscape evolution in southern Amazonia. Earth Surface Dynamics 2:493–511.

Magnusson, W. E., T. M. Sanaiotti, A. P. Lima, L. A. Martinelli, R. L. Victoria, M. C. Araújo, and A. L. Albernaz. 2002. A comparison of $\delta^{13}C$ ratios of

surface soils in savannas and forests in Amazonia. Journal of Biogeography 29:857–866.

Maia, R. G., H. K. Godoy, H. S. Yamaguti, P. A. Moura, and F. S. Costa. 1977. Projeto carvão no Alto Amazonas. Final report. CPRM, Rio de Janeiro, Brazil.

Malhi, Y., S. Adu-Bredu, R. A. Asare, S. L. Lewis, and P. Mayaux. 2013. African rainforests: past, present and future. Philosophical Transactions of the Royal Society of London Series B: Biological Sciences 368:20120312.

Martin, P., J. Martin, F. Q. Brearley, R. R. Ribbons, E. R. Lines, and A. L. Jacob. 2016. Can we set a global threshold age to define mature forests? PeerJ 4: e1595.

Martins, G. C., M. M. Ferreira, N. Curi, A. C. T. Vitorino, and M. L. N. Silva. 2006. Campos nativos e matas adjacentes da raegião de Humaitá (AM): atributos diferenciais dos solos. Ciência e Agrotectnologia 30:221–227.

Maslin, M. A., and S. J. Burns. 2000. Reconstruction of the Amazon Basin effective moisture availability over the past 14,000 years. Science 290:2285–2287.

Mayle, F. E., R. Burbridge, and T. J. Killeen. 2000. Millennial-scale dynamics of southern Amazonian rain forests. Science 290:2291–2294.

Mayle, F. E., and M. J. Power. 2008. Impact of a drier Early–Mid-Holocene climate upon Amazonian forests. Philosophical Transactions of the Royal Society of London Series B: Biological Sciences 363:1829–1838.

Meyers, P. A. 1997. Organic geochemical proxies of paleoceanographic, paleolimnologic, and paleoclimatic processes. Organic Geochemistry 27:213–250.

Middendorp, R. S., M. Vlam, K. T. Rebel, P. J. Baker, S. Bunyavejchewin, and P. A. Zuidema. 2013. Disturbance history of a seasonal tropical forest in western Thailand: a spatial dendroecological analysis. Biotropica 45:578–586.

Murray, A. S., and A. G. Wintle. 2003. The single aliquot regeneration dose protocol: potential for improvements in reliability. Radiation Measurements 37:377–381.

Nelson, B. W., V. Kapos, J. B. Adams, W. J. Oliveira, O. P. G. Braun, and I. L. Amaral. 1994. Forest disturbance by large blowdowns in the Brazilian Amazon. Ecology 75:853–858.

Newbery, D. M., X. M. van der Burgt, M. Worbes, and G. B. Chuyong. 2013. Transient dominance in a central African rainforest. Ecological Monographs 83:339–382.

Nock, C. A., D. J. Metcalfe, and P. Hietz. 2016. Examining the influences of site conditions and disturbance on rainforest structure through tree ring analyses in two Araucariaceae species. Forest Ecology and Management 366:65–72.

Norden, N., et al. 2015. Successional dynamics in neotropical forests are as uncertain as they are predictable. Proceedings of the National Academy of Sciences USA 112:8013–8018.

Ogrinc, N., G. Fontolanb, J. Faganelic, and S. Covellib. 2005. Carbon and nitrogen isotope compositions of organic matter in coastal marine sediments (the Gulf of Trieste, N Adriatic Sea): indicators of sources and preservation. Marine Chemistry 95: 163–181.

Ometto, J., J. R. Ehleringer, T. F. Domingues, J. A. Berry, F. Y. Ishida, E. Mazzi, N. Higucji, L. B. Flanagan, G. B. Nardoto, and L. Z. Martinelli. 2006. The stable carbon and nitrogen isotopic composition of vegetation in tropical forests of the Amazon Basin, Brazil. Biogeochemistry 79:251–274.

Patton, J. L., M. N. Silva, and J. R. Malcolm. 2000. Mammals of the Rio Juruá and the evolutionary and ecological diversification of Amazonia. American Museum of Natural History Bulletin 244:1–306.

Peng, J., Z. B. Dong, F. Q. Han, H. Long, and X. J. Liu. 2013. R package numOSL: numeric routines for optically stimulated luminescence dating. Ancient TL 31:41–48.

Pessenda, L. C. R., R. Boulet, R. Aravena, V. Rosolen, S. E. M. Gouveia, A. S. Ribeiro, and M. Lamotte. 2001. Origin and dynamics of soil organic matter and vegetation changes during the Holocene in a forest–savanna transition zone, southern Amazon State, Brazilian Amazon region. Holocene 11:250–254.

Pitman, N. C., et al. 2008. Three community change across 700 km of lowland Amazonian forest from the Andean foothills to Brazil. Biotropica 40:525–535.

Radambrasil. 1978. Folha SB. 20 Purus: geologia, geomorfologia, pedologia, vegetação, uso potencial da terra. DNPM 24034 (17). Departamento Nacional de Pesquisas Minerais, Rio de Janeiro, Rio de Janeiro, Brazil.

Reimer, P. J., et al. 2013. IntCal13 and Marine13 radiocarbon age calibration curves 0–50,000 years cal BP. Radiocarbon 55:1869–1887.

Rossetti, D. F., F. C. Alves, and M. M. Valeriano. 2017. A tectonically-triggered late Holocene seismite in the southern Amazonian lowlands, Brazil. Sedimentary Geology 358:70–83.

Rossetti, D. F., M. C. L. Cohen, T. C. Bertani, E. H. Hayakawa, J. D. S. Paz, D. F. Castro, and Y. Friaes. 2014. Late Quaternary fluvial terrace evolution in the main southern Amazonian tributary. Catena 116:19–37.

Rossetti, D. F., M. C. L. Cohen, and L. C. R. Pessenda. 2016. Vegetation change in southwestern Amazonia (Brazil) and relationship to the Late Pleistocene and Holocene climate. Radiocarbon 59:69–89.

Rossetti, D. F., P. M. Toledo, H. M. Moraes–Santos, and A. E. A. Santos Jr. 2004. Reconstructing habitats in Central Amazonia using megafauna, sedimentology, radiocarbon and isotope analysis. Quaternary Research 61:289–300.

Rossetti, D. F., et al. 2015. Mid-Late Pleistocene OSL chronology in western Amazonia and implications for the transcontinental Amazon pathway. Sedimentary Geology 330:1–15.

Rull, V. 2011. Neotropical biodiversity: timing and potential drivers. Trends in Ecology and Evolution 26:508–513.

Rull, V., T. Vegas-Vilarrubia, and E. Montoya. 2017. Paleoecology as a guide to landscape conservation and restoration in the neotropical Gran Sabana. Pages Magazine 25:82–83.

Sabatier, D., M. Grimaldi, M. F. Prevost, J. Guillaume, M. Godron, M. Dosso, and P. Curmi. 1997. The influence of soil cover organization on the floristic and structural heterogeneity of a Guianan rain forest. Plant Ecology 131:81–108.

Schwab, V. F., Y. Garcin, D. Sachse, G. Todou, O. Séné, J.-M. Onana, G. Achoundong, and G. Gleixner. 2015. Effect of aridity on $\delta^{13}C$ and $\delta D$ values of $C_3$ plant- and $C_4$ graminoid-derived leaf wax lipids from soils along an environmental gradient in Cameroon (Western Central Africa). Organic Geochemistry 78:99–109.

Scoles, R., and R. Gribel. 2011. Population structure of Brazil nut (Bertholletia excelsa, Lecythidaceae) stands in two areas with different occupation histories in the Brazilian Amazon. Human Ecology 39:455–464.

Scoles, R., and R. Gribel. 2015. Human influence on the regeneration of the Brazil nut tree (Bertholletia excelsa Bonpl., Lecythidaceae) at Capanã Grande Lake, Manicoré, Amazonas, Brazil. Human Ecology 43:843–854.

Shackleton, N. J. 1969. The last interglacial in the marine and terrestrial records. Proceedings of the Royal Society of London B 174:135–154.

Souza–Filho, P. W. M., M. L. E. S. Quadros, J. E. Scandolara, E. P. S. Filho, and M. R. Reis. 1999. Compartimentação morfoestrutural e neotectônica do sistema fluvial Guaporé–Mamoré–Alto Madeira, Rondônia, Brasil. Revista Brasileira de Geociências 29:469–476.

Stuiver, M., P. J. Reimer and R. W. Reimer. 2018. CALIB 7.1 [WWW program]. http://calib.org, accessed 2018-9-26

Tanner, E. V. J., F. Rodriguez-Sanchez, J. R. Healey, R. J. Holdaway, and P. J. Bellingham. 2014. Long-term hurricane damage effects on tropical forest tree growth and mortality. Ecology 95:2974–2983.

Tassinari, C. C. G., and M. J. B. Macambira. 1999. Geochronological provinces of the Amazonian Craton. Episodes 22:174–182.

ter Steege, H., V. Jetten, M. Polak, and M. Werger. 1993. Tropical rain forest types and soils of a watershed in Guyana, South America. Journal of Vegetation Science 4:705–716.

ter Steege, H., et al. 2006. Continental-scale patterns of canopy tree composition and function across Amazonia. Nature 443:444–447.

Toledo, M. B., and M. B. Bush. 2008. A Holocene pollen record of savanna establishment in coastal Amapá. Anais da Academia Brasileira de Ciências 80:341–351.

van der Hammen, T., and M. L. Absy. 1994. Amazonia during the last glacial. Palaeogeography, Palaeoclimatology, Palaeoecology 109:247–261.

Vlam, M., P. Sleen, P. Groenendijk, and P. A. Zuidema. 2017. Tree age distributions reveal large-scale disturbance-recovery cycles in three tropical forests. Frontiers in Plant Science 7:1–12.

Wang, X., R. L. Edwards, A. S. Auler, H. Cheng, X. Kong, Y. Wang, F. W. Cruz, J. A. Dorale, and H.-W. Chiang. 2017. Hydroclimate changes across the Amazon lowlands over the past 45,000 years. Nature 541:204–207.

Wilson, G. P., A. L. Lamb, M. J. Leng, S. Gonzalez, and D. Huddart. 2005. Variability of organic $\delta^{13}C$ and C/N in the Mersey Estuary, U.K. and its implications for sea-level reconstruction studies. Estuarine, Coastal and Shelf Science 64:685–698.

Wittmann, F., E. Householder, M. T. Piedade, R. L. Assis, J. Schöngart, P. Parolin, and W. J. Junk. 2013. Habitat specificity, endemism and the neotropical distribution of Amazonian white-water floodplain trees. Ecography 36:690–707.

Wright, S. J. 2005. Tropical forests in a changing environment. Trends in Ecology and Evolution 20:553–560.

Zemp, D. C., C.-F. Schleussner, H. M. J. Barbosa, M. Hirota, V. Montade, G. Sampaio, A. Staal, L. Wang-Erlandsson, and A. Ramming. 2017. Self-amplified Amazon forest loss due to vegetation-atmosphere feedbacks. Nature Communications 8:14681.

## SUPPORTING INFORMATION

Additional Supporting Information may be found online at: http://onlinelibrary.wiley.com/doi/10.1002/ecs2.2457/full